Energy Conversion and Management 171 (2018) 1116–1133

Contents lists available at ScienceDirect

Energy Conversion and Management

journal homepage: www.elsevier.com/locate/enconman

Multi-objective optimization of biomass-based solid oxide fuel cell integrated with Stirling engine and electrolyzer

Ali Habibollahzade, Ehsan Gholamian, Ehsan Houshfar*, Amirmohammad Behzadi

School of Mechanical Engineering, College of Engineering, University of Tehran, P.O. Box 11155-4563, Tehran, Iran

ARTICLE INFO

Keywords:
Solid oxide fuel cell
Stirling
Multi-objective optimization
Gasification
Anode/cathode recycle
Electrolyzer

ABSTRACT

The aim of this study is to increase the power generation/exergy efficiency and reduce total product cost/environmental contamination of solid oxide fuel cells. Accordingly, three integrated systems are proposed and analyzed from energy, exergy, exergoeconomic, and environmental viewpoints through the parametric study. The first model assesses the combination of a gasifier with a solid oxide fuel cell. In the second model, waste heat of the first model is reused in the Stirling engine to enhance the efficiency and power generation. The last model proposes reuse of the surplus power of the Stirling engine in a proton exchange membrane electrolyzer for hydrogen production. Considering total product cost, exergy efficiency, and hydrogen production rate as the objective functions, a multi-objective optimization is applied based on the genetic algorithm. The results indicate that at the optimum operating condition, the exergy efficiency of the model (a), (b), and (c) is 28.51%, 39.51%, and 38.03%, respectively. Corresponding values for the energy efficiency and the emission rate of the models are 31.13%, 67.38%, 66.41%, 1.147 t/MWh, 0.7113 t/MWh, 0.7694 t/MWh. At the optimum solution point, total product cost associated with the model (a), (b), and (c) is 19.33 $/GJ, 18.91 $/GJ, and 24.93 $/GJ, respectively. If the hydrogen production rate and total product cost considered as the objective functions, at optimum solution point, the rate of hydrogen production and overall product cost would be 56.5 kg/day and 41.76 $/GJ, respectively. Overall, the proposed integrated systems demonstrate decent functionality both in thermodynamic, environmental, and economic aspects.

1. Introduction

Nowadays, by increasing demand for higher power generation and issues related to global warming, researchers have shown an increased interest in designing more efficient power plants. Optimizing a power plant could be accomplished by various approaches, e.g., waste heat recovery, economic aspects, and increase in exergetic efficiency. Waste heat recovery is feasible by combining two or more power plants, i.e., connecting smaller scale power plants with higher scale ones can increase exergetic efficiency thus achieve higher power output [1]. Accordingly, designing an integrated high-efficiency power plant while minimizing the total product cost is one of the most critical topics of thermal design optimization.

1.1. Biomass gasification based solid oxide fuel cell

Gasification has for a long time been used to produce syngas from various solid fuel sources including biomass and municipal waste [1]. This method is expected to provide higher syngas with low emission rates compared to the other processes, i.e., pyrolysis, combustion, and fermentation [2].

Fuel cells are highly efficient electrochemical systems to convert chemical bonds energy into electricity. Fuel and oxygen react in the anode/cathode and thereafter produce clean electricity with very low NO_x and SO_x emissions. Using fuel cells is deemed a decent choice in transportation and aviation sector since they are expected to operate without any vibration and noise. SOFCs are among the most efficient types of fuel cells, which can directly produce electricity from the fuel. Other main advantages of SOFC are: they are fuel flexible, suitable for any combined system for hydrogen/power/cooling or heating generation [3]. On the other hand, some important disadvantages of SOFCs are: cell components may break down due to high operating temperature, high chance of corrosion, and long startup time [3].

Some biomass gasification based SOFC integrated plants are proposed by various researchers, focusing on the design and optimization of such systems. Ghaffarpour et al. [4] proposed a biomass-based SOFC integrated with gas turbine and Rankine cycle. The results indicate that the current density and biomass feeding rate are the major effective

* Corresponding author.
E-mail address: houshfar@ut.ac.ir (E. Houshfar).

https://doi.org/10.1016/j.enconman.2018.06.061
Received 26 March 2018; Received in revised form 18 May 2018; Accepted 16 June 2018

Nomenclature

A	area, m^2
c	specific exergy cost, $/GJ
$\dot{C}$	cost rate, $/h
$\dot{E}$	exergy rate, kW
f	exergoeconomic factor
F	Faraday constant, C/mol
$\Delta\overline{g}^0$	change in molar Gibbs free energy, J/mol
h	enthalpy
i_r	interest rate
j	current density, A/m^2
J	PEME current density
K	equilibrium constant
LHV_f	fuel lower heating value
M	molar mass
$\dot{m}_f$	fuel mass flow rate
N	operating hours, hr
$n_1,n_2,\ldots,n_7$	mole number of reaction components
n_e	number of electrons produced per hydrogen mole
$\dot{n}$	molar flow rate
N_C	number of cells in the stack
P	pressure
PR	pressure ratio
p_{H_2O}	partial pressure of H_2O
p_{H_2}	partial pressure of H_2
p_{O_2}	partial pressure of O_2
$\dot{Q}_{high}$	heat rate of the heater inside the Stirling engine, kW
$\dot{Q}_{loss}$	heat loss rate of cooler inside the Stirling engine, kW
r	relative cost difference (%)
R	total ohmic resistance
R_{AR}	anode recycling ratio
R_{CR}	cathode recycling ratio
$\overline{R}$	universal gas constant, J/mol K
RV	piston compression ratio of the Stirling engine
s	specific entropy
T	temperature
T_g	gasification temperature
U_f	fuel utilization ratio
V	voltage, V
V_0	reversible potential
V_C	cell voltage, V
V_{loss}	loss voltage, V
V_N	reversible cell voltage, V
w	mole fraction of moisture in the biomass (kmol/kmol)
$\dot{W}$	power, kW
y_i	molar fraction
y_r	extent of water gas shift reaction, mol/s
x_r	extent of steam reforming reaction for methane, mol/s
$\dot{Z}$	cost rate of components, $/h
$\dot{Z}^{CI}$	capital investment cost rate of components, $/h
$\dot{Z}^{OM}$	operating and maintenance cost rate of components, $/h

Superscripts

ch	chemical
ph	physical

Subscripts and abbreviations

0	dead state
act	activation
AB	afterburner
AC	air blower
an	anode
AHX	air heat exchanger
ca	cathode
CEPI	chemical engineering plant cost index
conc	concentration
CRF	capital recovery factor
D	destruction
e	electrolyte
FC	fuel blower
FHX	fuel heat exchanger
HS, gas	highest stirling gas temperature
i	inlet
INV	DC to AC inverter
k	k^{th} component
L	Loss
LS, gas	lowest stirling gas temperature
MC	moisture content
MOO	multi-objective optimization
o	outlet
ohm	ohmic
P	pump/Product
PEME	proton exchange membrane electrolyzer
PY	present year
R	reforming
S	shifting
SOFC	solid oxide fuel cell
SE	Stirling engine
tot	total

Greek letters

η_{pcy}	polytrophic efficiency
$\eta_{mech,SE}$	Stirling engine mechanical efficiency
ε	emission indicator
ε_{SE}	heater efficiency inside the Stirling engine
ζ	lowest to highest temperature of Stirling engine
γ	ratio of specific heats
η_I	energy efficiency
η_{II}	exergy efficiency
φ	maintenance factor
τ	annual plant operation hours
σ	total ionic conductivity
λ	content of water

parameters and at an SOFC temperature of 983 K, the exergy efficiency is 22.7%. Lorenzo and Fragiacomo [5] performed an energy analysis of a biomass-based SOFC system and Speidel et al. [6] analyzed biomass-based SOFC system by combined gasification and fermentation. Gholamian et al. [7] suggested and analyzed the integration of a gasifier with an SOFC system for cooling, heating, and power generation purposes. The results showed that the exergy efficiency of the proposed method would increase up to 49.88% compared to the solo SOFC. Mortazaei and Rahimi [8] compared two biomass based SOFC systems from thermodynamic and environmental viewpoints. The results indicate that digester based SOFC has higher energy efficiency by 11.1% while lower contamination by 19.3%. Tan et al. [9] analyzed a hybrid system consisting of an SOFC, biomass gasification, gas expanders and Kalina cycle, stating that for the base case model, total exergy

destruction is around 397 kW and the efficiency of the hybrid system can reach up to 64.2%.

1.2. Stirling engine and waste heat recovery of SOFC

SOFCs usually operate at high temperatures and therefore their waste heat is too high; hence such waste heat can be recovered in a bottom cycle or engine to further improve the system efficiency [1]. Stirling engine (SE) is, on the other hand, an external combustion engine which can make use of various external heat sources to produce electricity. SEs operate based on a closed regenerative cycle with different working fluids, e.g., helium, nitrogen, hydrogen, or air. Quietness, ease of use of any heat source, no pollutant emissions, and high efficiency are the main advantages of SEs [10].

Exploiting exhaust gases of the SOFC as a heat source of SE would increase power production and efficiency. Analyzing and optimizing fuel cells and combining them with SEs or other power plants is also proposed by many researchers. Gholamian et al. [1] investigated two combined power plants for waste heat recovery: SOFC/Kalina and SOFC/ORC. They have reported that the SOFC/ORC integrated system has higher exergy efficiency (62.3%) than SOFC/Kalina (59.5%). Rokni [11] analyzed a municipal solid waste gasification system–SOFC–SE integrated plant to reuse the off-gases of the SOFC stack. Results indicated that the combined plant can increase electricity production by up to 50%. Entezari et al. [12] proposed a combination of a gas turbine with an SE to enhance the power generation and exergy efficiency. The results revealed that the combination would increase the exergy efficiency by 16.1% and reduce levelized electricity cost by 10.3%. In another study, Rokni [13] investigated exergoeconomic and thermodynamic of the SE-biomass gasifier and SOFC hybrid system. He reported electricity generation and hot water may cost 0.1204 $/kWh and 0.0214 $/kWh, respectively. Sowale et al. [14] implemented an SE to recover the waste heat of a combustor. The results indicate that via 820 W available heat rate, the SE's power output would be 27 W. Ranjbar et al. [15] proposed and analyzed a trigeneration system by the integration of SOFC/Kalina and SOFC/organic Rankine cycle (ORC). Their results indicated that the trigeneration system can reach 33% higher energy efficiency than the standalone SOFC. Hosseinpour et al. [16] analyzed energy and exergy of SOFC/SE hybridization plant, where they indicated that combination of the proposed systems can increase energy efficiency up to 24.61% and it can reach 76.32%. Xu et al. [17] analyzed the combination of an SE for the power enhancement of a direct carbon SOFC plant. They stated that by increasing the SOFC inlet temperature, exergy efficiency of the proposed system reaches 56.44%. Rokni [18] introduced SOFC/SE 10 kW integrated plants for a family home, stating that the total power output of the hybrid plant is 10% higher than a standalone SOFC or SE.

1.3. Proton exchange membrane electrolyzer

A considerable attention is paid to hydrogen production recently, as it is one of the most suitable energy resources for the future due to its low emission. Three major types of fuel cells (along with SOFC) are molten carbonate (MCFC), phosphoric acid (PAFC) and proton exchange membrane (PEMFC). Other types of fuel cells e.g. alkaline and direct methanol can be implemented in transportation. Main advantages of PAFC are: achievable heating and power generation and low sensitivity to fuel impurity [19]. The main disadvantages of this type of fuel cell are: the low current density, low power generation, and long startup time [19]. The advantages and disadvantages of MCFCs are: high efficiency, the flexibility of fuel, suitable for heat and power generation, long startup time, low power and high corrosion risk [20]. PEMFCs have some important advantages over previously mentioned FCs: quick startup, less corrosion issues, low operating temperature. The major disadvantages of PEMFCs are: high sensitivity to fuel impurity and costly catalysts [21]. Additionally, proton exchange membrane electrolyzer (PEME) as a hydrogen production unit has many advantages such as high voltage efficiency at higher current densities, better dynamic operation, and compact design [22]. Accordingly, in this study, PEME is implemented for hydrogen production. Combining PEME systems with various energy systems has been extensively studied.

Nami et al. [23] tried to recover waste heat of a gas turbine to exploit in an ORC cycle and also for hydrogen production purpose using PEME. The results revealed that exergy efficiency and rate of hydrogen production would be 49.21% and 56.2 kg/h, respectively. In a later study, Nami and Akrami [24] analyzed exergy and exergoeconomic aspects of a hybrid system consisting of a gas turbine and a PEME. They concluded that exergy efficiency and rate of hydrogen production of the hybrid system are 52.09% and 8.723 kg/h, respectively. Moradi Nafchi et al. [25] investigated an integrated system incorporating a PEME, concentrating solar system and a thermal storage. The results indicated that hydrogen and efficiency of electricity production of the system are 23.1% and 45%, respectively. Boyaghchi et al. [26] proposed a multi-generation system consisting of dual ORC, a PEME and a biomass gasification unit. The optimization results indicated that hydrogen cost and environmental contamination can be reduced by 49.18% and 34.58%, respectively. Ferrero and Santarelli [27] investigated a concept incorporating multi-junction solar cells integrated with a PEME. The results showed that the integrated system has higher efficiency by 12% compared to stand-alone PEME.

1.4. Multi-objective optimization

Few researchers further tried to optimize the SOFC based systems by MOO technique. Sadeghi et al. [28] optimized a syngas fed cogeneration SOFC system by MOO method. The optimization results showed that minimization of the total product cost of the system leads to a higher CO2 emission and lower values of exergy efficiency of the system. In a recent study, Sharma et al. [29] applied an MOO to optimize the conflicting objectives of a biomass based SOFC. The results indicated less sensitivity of robust MOO compared to normal MOO method. Shamoushaki et al. [30] performed exergy, exergoeconomic, environmental analysis and MOO of an SOFC/gas turbine system. The results demonstrated that at optimum solution point, total cost rate and exergy efficiency of the system is 0.0435 $/s and 57.7%, respectively. Hajabdollahi and Fu [31] further optimized SOFC/gas turbine system by MOO technique. Optimization results revealed that at the optimum design point, exergy efficiency and total cost rate of the system may be 826.1 $/h and 48.2%, respectively. Aminyavari et al. [32] analyzed an SOFC/gas turbine integrated with Rankine cycle from a thermodynamic viewpoint. Subsequently, they optimized the system by MOO method. The results showed that at the optimal solution point, exergy efficiency and overall cost rate of the system would be 65.11% and 0.137 €/s.

Comprehensive literature review reveals that the scientific literature lacks energy, exergy, exergoeconomic, environmental analysis and MOO of biomass-based SOFC integrated with SE and PEME. In the present study, a gasifier combined with an SOFC with anode and cathode gas recycling unit, an SE, a PEME is investigated from thermodynamic viewpoints. The integration is proposed through two scenarios: (1) Biomass gasifier is employed as the SOFC feeder and an SE is established to recover the waste heat of SOFC to enhance the power production and (2) surplus power, which is generated by SE, is used in a PEME for hydrogen production. Exergy, exergoeconomic, environmental analysis and parametric study of the proposed systems are performed and compared to each other, and the proposed cycles are optimized by the MOO technique.

Main objectives and novelties of this research may be summarized as:

- Two new integrated systems are proposed along with conventional biomass-based SOFC: (1) SOFC integrated with SE and (2) SOFC

integrated with SE and PEME.

- Comparing energy, exergy, environmental, and exergoeconomic aspects of the proposed systems
- Appling an MOO to all models by altering effective parameters to minimize total specific product cost, and maximize exergetic efficiency/hydrogen production rate
- Ascertaining optimum values of the crucial parameters and the objective functions
- Gathering the optimal solution points as Pareto frontiers and analyzing scatter distribution of the effective parameters of each system

2. System description and assumptions

Schematic diagram of the proposed systems is illustrated in Fig. 1. Model (a) is assumed as biomass gasifier (as the feeder) combined with SOFC. The waste heat of the Model (a) is reused in an SE to enhance the exergy efficiency/power generation (Model (b)). In the last proposed model (Model (c)), the surplus power which is produced by the SE is used in a PEME for hydrogen production.

The gasifier prepares the required fuel for the SOFC, and the SE is chosen as the bottom system to generate power and provide warm water from the waste heat recovery process. Ambient air is firstly blown into an air heat exchanger (AHX) by an air blower (points 1 and 2). Afterward, the air is mixed with recirculated cathode off-gases at mixing unit and enters the cathode (points 3a, 3b, and 3). Air and biomass are fed into the gasifier (points 5 and 6) and then syngas is blown into the mixer by a fuel blower. Recirculated anode exhaust gases are mixed with blown fuel and enter the anode section (points 7, 8, 9b, and 9). Following electrochemical reactions in the SOFC, unburned anode and cathode gases burn in the afterburner, and hot exhaust gases pass through the AHX, respectively (points 10b, 4a, and 11).

The exhaust SOFC flue gases are hot enough to be exploited in the SE, so the off-gases are reused as a heat source of the SE and then is discharged to the environment (points 12 and 13). The cooling water passing through the SE is warm enough, so a room heater is implemented to prepare warm water for a family home (point 14). The cooling water after heat exchanged in the room heater is yet pumped again to the SE (point 15).

Generated power by SE is used in the PEME. Heater heats up the water (point 16) and hot water enters the PEME to split water molecules into hydrogen and oxygen (state 17, 18 and 19). Oxygen separation unit separates the oxygen molecules and remaining water recirculates in the cycle.

Some assumptions are considered to simplify the analysis:

- All gases are treated as an ideal gas, and molar composition of air is presumed with 21% N_2 and 79% O_2.
- Thermodynamic equilibrium and steady-state condition are assumed during the analyses.
- The produced syngas is in thermodynamic equilibrium.
- Kinetic and potential energy changes are omitted.
- All components are thermally insulated, so the heat loss is neglected.
- No contact resistance in the SOFC.
- Unburned gases of SOFC are fully oxidized in the afterburner.

3. Methods

Energy, exergy, exergoeconomic, and environmental of the proposed integrated systems are analyzed and described in this section. The Engineering equation solver (EES) package is implemented to solve the correlated equations of energy, exergy, and exergoeconomic and thereafter evaluate the integrated systems.

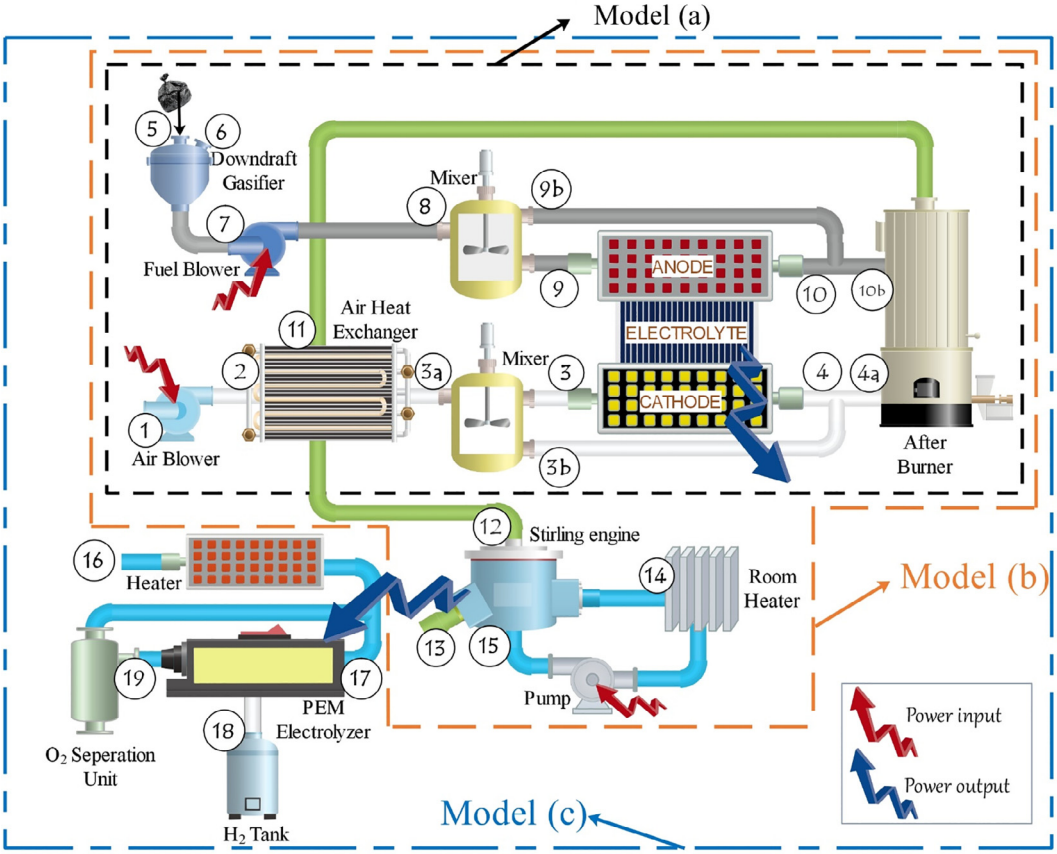

Fig. 1. Schematic diagram of the proposed systems: model (a): Gasifier/SOFC, model (b): Gasifier/SOFC/SE, model (c): Gasifier/SOFC/SE/PEME.

3.1. Energy and exergy analysis

The energy analysis is based on the energy balance for each component:

$$\dot{Q}-\dot{W} = \sum \dot{m}_{out} h_{out} - \sum \dot{m}_{in} h_{in} \quad (1)$$

Additionally, exergy destruction rate for each component is obtained from:

$$\dot{E}_D = \sum \dot{E}_{in} - \sum \dot{E}_{out} \quad (2)$$

in which exergy rate consists of chemical and physical exergy.

3.1.1. The gasifier

Downdraft gasifier produces the syngas with low tar and also is suitable for small and medium systems [7]. Hence in this study, downdraft gasifier is selected as the SOFC feeder. In modeling of the downdraft gasifier, the equilibrium model is assumed supposing that all the reactions are in thermodynamic equilibrium and the syngas burns and achieves balance before leaving the gasifier. The gasification elementary reactions are [7,33]:

$$C + CO_2 \leftrightarrow 2CO \quad (3)$$

$$C + H_2O \leftrightarrow CO + H_2 \quad (4)$$

$$C + 2H_2 \leftrightarrow CH_4 \quad (5)$$

$$CO + H_2O \leftrightarrow CO_2 + H_2 \quad (6)$$

In addition, the global reaction for the gasification is assumed as [34]:

$$CH_aO_bN_c + wH_2O + n_1(O_2 + 3.76N_2) \rightarrow n_2H_2 + n_3CO + n_4CO_2 + n_5H_2O + n_6CH_4 + n_7N_2 \quad (7)$$

where $CH_aO_bN_c$ is the fuel chemical formula, w is the moisture content of biomass, and n_1 is the kmol of oxygen. Also, n_2 to n_7 can be determined using the mass balance for C, H, O, and N. The ultimate analysis of municipal solid waste is 47.6% C, 6% H, 1.2% N, 0.3% S, 32.9% O and 12% Ash with higher heating value of 433034 kJ/kmol and moisture content of 20% [35]. The MC is expressed as [36]:

$$\mathrm{MC} = \frac{\text{mass of water}}{\text{mass of wet biomass}} \times 100 \quad (8)$$

So w can be found from [37]:

$$w = \frac{M_{biomass} MC}{18(1-MC)} \quad (9)$$

Considering achievable equilibrium where remaining solid carbon is negligible, the equilibrium constants for the elementary reactions of hydrogasification (reaction (5) and water–gas shift (reaction (6)) are respectively defined as [33]:

$$K_1 = \frac{n_6}{n_2^2}\left(\frac{P/P_0}{n_{tot}}\right)^{-1} \quad (10)$$

$$K_2 = \frac{n_2 n_4}{n_3 n_5}\left(\frac{P/P_0}{n_{tot}}\right)^{0} \quad (11)$$

where the equilibrium constants can be determined from the Gibbs function minimization [33]:

$$\frac{-\Delta G_1^0}{\bar{R}T_g} = LnK_1 \quad (12)$$

$$\frac{-\Delta G_2^0}{\bar{R}T_g} = LnK_2 \quad (13)$$

where T_g is the gasification temperature.

$$-\Delta G_1^0 = (\bar{h}_{CH_4} - T_g \bar{s}^0_{CH_4}) - 2(\bar{h}_{H_2} - T_g \bar{s}^0_{H_2}) \quad (14)$$

$$-\Delta G_2^0 = (\bar{h}_{CO_2} - T_g \bar{s}^0_{CO_2}) + (\bar{h}_{H_2} - T_g \bar{s}^0_{H_2}) - (\bar{h}_{CO} - T_g \bar{s}^0_{CO}) - (\bar{h}_{H_2O} - T_g \bar{s}^0_{H_2O}) \quad (15)$$

Since the gasification is assumed adiabatic, by implementing the energy balance for the gasifier, the air–fuel ratio can be found:

$$\bar{h}^0_{f-biomass} + w \times \bar{h}^0_{f-H_2O} = n_2(\bar{h}^0_{f-H_2} + \Delta\bar{h}_{H_2}) + n_3(\bar{h}^0_{f-CO} + \Delta\bar{h}_{CO}) + n_4(\bar{h}^0_{f-CO_2} + \Delta\bar{h}_{CO_2}) + n_5(\bar{h}^0_{f-H_2O} + \Delta\bar{h}_{H_2O}) + n_6(\bar{h}^0_{f-CH_4} + \Delta\bar{h}_{CH_4}) + n_7(\bar{h}^0_{f-N_2} + \Delta\bar{h}_{N_2}) \quad (16)$$

3.1.2. The solid oxide fuel cell system

Internal or external reformer can be employed for the SOFC system. In the present study, an internal reformer is used because of its higher potential for additional cooling of the SOFC stack and also its lower price compared to the external reforming technique [15].

Reforming and shifting reactions which occur at the cathode and anode sides of SOFC are:

$$x_r \rightarrow (CH_4 + H_2O \rightarrow CO + 3H_2)(reforming) \quad (17)$$

$$y_r \rightarrow (CO + H_2O \rightarrow CO_2 + H_2)(shifting) \quad (18)$$

Absorbing H_2 and conducting O_2 (electrochemical reaction) as given by Eq. (19) takes place in a single cell [38]:

$$z_r \rightarrow \left(H_2 + \frac{1}{2}O_2 \rightarrow H_2O\right)(overall\ reaction) \quad (19)$$

The equilibrium constants for the reforming and shifting reactions which take place in the internal reformer of the SOFC are calculated as follows [7]:

$$\ln K_R = -\frac{\Delta g_R^{-0}}{\bar{R}T_{FC,e}} = \ln\left[\frac{(\dot{n}_{CO} + x_r - y_r) \times (\dot{n}_{H_2} + 3x_r + y_r - z_r)}{(\dot{n}_{CH_4} + x_r) \times (\dot{n}_{H_2O} - x_r - y_r + z_r)} \times \frac{P^2}{n^2_{tot,in} + 2x_r}\right] \quad (20)$$

$$\ln K_S = -\frac{\Delta g_s^{-0}}{\bar{R}T_{FC,e}} = \ln\left[\frac{(\dot{n}_{CO_2} + y_r) \times (\dot{n}_{H_2} + 3x_r + y_r - z_r)}{(\dot{n}_{CO} + x_r - y_r) \times (\dot{n}_{H_2O} - x_r - y_r + z_r)}\right] \quad (21)$$

where x_r and y_r are the molar conversion rates of the reforming and shifting reactions. The current density can be expressed by Faraday's law [38]:

$$j = \frac{n_e F z_r}{N_c A_c} \quad (22)$$

where A_c denotes the active cell area, N_c indicates the number of stack cells, F is the Faraday constant, and $n_e = 2$ is the number of electrons being generated per mole of hydrogen.

Amount of reacted H_2 in the electrochemical reaction is calculated using the fuel utilization factor (U_f) equation:

$$U_f = \frac{z_r}{\dot{n}_{H_2} + 3x_r + y_r} \quad (23)$$

Accordingly, the power output of the SOFC stack ($\dot{W}_{SOFC,stack,AC}$) can be calculated as follows [15]:

$$\dot{W}_{SOFC,stack,DC} = N_c A_c j V_c \quad (24)$$

$$\dot{W}_{SOFC,stack,AC} = \dot{W}_{SOFC,stack,DC} \times \eta_{inv} \quad (25)$$

The net power output of the SOFC is then obtained by subtracting power consumptions of the air and fuel blowers from the SOFC stack power output:

$$\dot{W}_{SOFC} = \dot{W}_{SOFC,stack,AC} - \dot{W}_{FC} - \dot{W}_{AC} \quad (26)$$

In Eq. (27), V_c is the cell voltage given by:

$$V_c = V_N - V_{loss} \tag{27}$$

V_N defines as the reversible cell voltage which can be obtained from the Nernst equation [39]:

$$V_N = -\frac{\Delta G^0}{n_e F} - \frac{\overline{R} T_C}{n_e F} ln\left(\frac{p_{H_2O}}{p_{H_2}\sqrt{p_{O_2}}}\right) \tag{28}$$

where T_C denotes the operating temperature of the SOFC, ΔG^o is the change in molar Gibbs free energy and p_{H_2}, p_{O_2}, and p_{H_2O} are partial pressures of H_2, O_2, and H_2O, respectively. Also, V_{loss} denotes polarization losses and is defined as:

$$V_{loss} = V_{ohm} + V_{act} + V_{conc} \tag{29}$$

Additional equations needed to solve the activation, ohmic/concentration polarization, and other electrochemical equations can be found in the literature [15,40–42].

3.1.3. The Stirling engine

Ideal Stirling cycle has four processes: external heat reservoir rises the working fluid temperature in an isochoric process, the piston then undergoes an isothermal expansion process. After exchanging heat with the regenerator and heat rejection to the cold reservoir in the second isochoric process, cooled down working fluid undergoes isothermal compression process and the cycle ends.

Since any heat source can be a hot reservoir for an SE, in this study the exhaust hot gases of SOFC are considered as the heat source. Hence, off-gases of SOFC are assumed as the high-temperature reservoir while water is taken as the low-temperature reservoir.

Instead of using ideal Stirling cycle, a pseudo-Stirling cycle is adopted, to be in better agreement with real engine data. In this case, the power output of the SE is defined as [13]:

$$\dot{W}_{SE} = \eta_{pcy}(\dot{Q}_{high} - \dot{Q}_{loss}) \tag{30}$$

where $\dot{Q}_{high}$ is the heat rate which SE absorbs from the SOFC exhaust gases, $\dot{Q}_{loss}$ is the rejected heat of the SE. Polytropic efficiency η_{pcy} can be calculated from [13]:

$$\dot{Q}_{loss} = \dot{Q}_{high}(1 - \eta_{mech,SE}) \tag{31}$$

$$\eta_{pcy} = \left[\frac{(1 - RV^{1-\gamma}) - \zeta(RV^{\gamma-1} - 1)}{(1 - RV^{1-\gamma}) + (1-\zeta)(1-\varepsilon_{SE})}\right] \tag{32}$$

where RV and ε_{SE} are piston compression ratio and efficiency of the heater inside the SE, respectively. γ is considered constant and equal to 1.667, and ζ is defined as the ratio of the minimum and the maximum temperature inside the Stirling cycle. ζ is a crucial parameter since it relies on various parameters e.g. type of working gas, the mass of gas inside the SE, the conductivity of piston, and other internal components. It is expressed as follows:

$$\zeta = \left[\frac{T_{LS,gas} + 273.15}{T_{HS,gas} + 273.15}\right] \tag{33}$$

$T_{HS,gas}$ and $T_{LS,gas}$ can be defined as [13]:

$$T_{HS,gas} = T_{heater,wall} - \Delta T_{high} \tag{34}$$

$$T_{cooler,wall} = T_{water,inlet} + \frac{2}{3}\Delta T_{water} \tag{35}$$

$$T_{LS,gas} = T_{cooler,wall} + \Delta T_{low} \tag{36}$$

where $T_{heater,wall}$ and $T_{cooler,wall}$ are the temperature of the heater wall (high-temperature reservoir) and cooler wall (low-temperature reservoir) inside the SE.

3.1.4. The proton exchange membrane electrolyzer

The theoretical energy required for electrolysis of water is defined as:

$$\Delta H = \Delta G + T\Delta S \tag{37}$$

where ΔG is Gibbs free energy and $T\Delta S$ is thermal energy. Hydrogen mass flow rate which is produced by the PEME can be calculated as [43]:

$$\dot{m}_{H_2,out} = \dot{m}_{H_2O,reacted} = \frac{J}{2F} \tag{38}$$

where J is the current density of the PEME and F is Faraday constant.

Electricity into the PEME is:

$$E_{electrical} = JV \tag{39}$$

V is PEME voltage:

$$V = V_0 + \eta_{act,an} + \eta_{act,ca} + \eta_{ohm} \tag{40}$$

where V_0 denotes reversible potential, $\eta_{act,an}$, $\eta_{act,ca}$ and η_{ohm}, refer to activation overpotential of the anode, activation overpotential of the cathode and the ohmic overpotential of the electrolyte respectively. Reversible potential expresses as [43]:

$$V_0 = 1.229 - 8.5 \times 10^{-4}(T_{PEME} - 298) \tag{41}$$

Furthermore, the local ionic conductivity of the membrane can be defined as [43]:

$$\sigma(\lambda(x)) = (0.5139\lambda(x) - 0.326) \times exp\left(1268 \times \left[\frac{1}{303} - \frac{1}{T}\right]\right) \tag{42}$$

where x refers to the membrane depth measured from cathode interface, and $\lambda(x)$ is the water content at distance of x. $\lambda(x)$ can be defined as follows:

$$\lambda(x) = (\lambda_{an} - \lambda_{ca})\frac{x}{l} + \lambda_{ca} \tag{43}$$

l is the thickness of the membrane, λ_{an} and λ_{ca} denote contents of water at anode and cathode-membrane interface, respectively.

Table 1
Exergy balance and exergy efficiency of components of the proposed systems.

Component	Exergy balance	Exergy efficiency
Downdraft gasifier	$\dot{E}_{D,G} = \dot{E}_5 + \dot{E}_6 - \dot{E}_7$	$\eta_{II,G} = \dot{E}_7/(\dot{E}_5 + \dot{E}_6)$
Fuel blower	$\dot{E}_{D,FC} = \dot{W}_{FC} - (\dot{E}_8 - \dot{E}_7)$	$\eta_{II,FC} = (\dot{E}_8 - \dot{E}_7)/\dot{W}_{FC}$
Air blower	$\dot{E}_{D,AC} = \dot{W}_{AC} - (\dot{E}_2 - \dot{E}_1)$	$\eta_{II,AC} = (\dot{E}_2 - \dot{E}_1)/\dot{W}_{AC}$
Air heat exchanger	$\dot{E}_{D,AHX} = \dot{E}_{11} - \dot{E}_{12} - (\dot{E}_{3a} - \dot{E}_2)$	$\eta_{II,AHX} = (\dot{E}_{3a} - \dot{E}_2)/(\dot{E}_{11} - \dot{E}_{12})$
Anode mixer	$\dot{E}_{D,AM} = \dot{E}_8 + \dot{E}_{9b} - \dot{E}_9$	$\eta_{II,AM} = (\dot{E}_9)/(\dot{E}_8 + \dot{E}_{9b})$
Cathode mixer	$\dot{E}_{D,CM} = \dot{E}_{3b} + \dot{E}_{3a} - \dot{E}_3$	$\eta_{II,CM} = (\dot{E}_3)/(\dot{E}_{3a} + \dot{E}_{3b})$
SOFC Stack	$\dot{E}_{D,SOFC} = \dot{E}_3 + \dot{E}_9 - (\dot{E}_4 + \dot{E}_{10}) - \dot{W}_{SOFC,stack,DC}$	$\eta_{II,SOFC,stack} = (\dot{E}_4 + \dot{E}_{10} + \dot{W}_{SOFC,stack,DC})/(\dot{E}_3 + \dot{E}_9)$
After burner	$\dot{E}_{D,AB} = \dot{E}_{4a} + \dot{E}_{10b} - \dot{E}_{11}$	$\eta_{II,AB} = (\dot{E}_{11})/(\dot{E}_{4a} + \dot{E}_{10b})$
Inverter	$\dot{E}_{D,INV} = \dot{W}_{SOFC,stack,DC} - \dot{W}_{SOFC,stack,AC}$	$\eta_{II,INV} = (\dot{W}_{SOFC,stack,AC})/(\dot{W}_{SOFC,stack,DC})$
Stirling engine	$\dot{E}_{D,SE} = \dot{E}_{12} - \dot{E}_{13} - (\dot{E}_{14} - \dot{E}_{15} + \dot{W}_{SE})$	$\eta_{II,SE} = (\dot{E}_{14} - \dot{E}_{15} + \dot{W}_{SE})/(\dot{E}_{12} - \dot{E}_{13})$
Pump	$\dot{E}_{D,P} = \dot{W}_P - (\dot{E}_{15} - \dot{E}_{14})$	$\eta_{II,P} = (\dot{E}_{15} - \dot{E}_{14})/(\dot{W}_P)$
PEME	$\dot{E}_{D,PEME} = \dot{W}_{PEME} - \dot{E}_{18} - (\dot{E}_{19} - \dot{E}_{17})$	$\eta_{II,PEME} = ((\dot{E}_{19} - \dot{E}_{17}) + \dot{E}_{18})/(\dot{W}_{PEME})$

Furthermore, total ohmic resistance can be determined as [43]:

$$R_{PEME} = \int_0^L \frac{dx}{\sigma(\lambda(x))} \tag{44}$$

Using ohmic's law, the ohmic overpotential is expressed as:

$$\eta_{ohm} = JR_{PEME} \tag{45}$$

The activity of the electrodes is measured by activation overpotential as follows [44]:

$$\eta_{act,i} = \frac{RT}{F}\sinh^{-1}\left(\frac{J}{2J_{0,i}}\right) = \frac{RT}{F}ln\left(\frac{J}{2J_{0,i}} + \sqrt{\left(\frac{J}{2J_{0,i}}\right)^2 + 1}\right) \tag{46}$$

$J_{0,i}$ is the exchange current density [44]:

$$J_{0,i} = J_i^{ref} exp\left(-\frac{E_{act,i}}{RT}\right) \tag{47}$$

where J_i^{ref} is the pre-exponential factor and $E_{act,i}$ is the activation energy for the anode and the cathode.

Accordingly, exergy balances and exergy efficiency for the components are tabulated in Table 1.

3.2. Exergoeconomic analysis

Various methods have been developed for exergoeconomic assessment, while specific costing theory (SPECO) has been extensively used to investigate economic aspects of the energy systems. The theory applies a method to determine cost rates and specific exergy costs of the components. The cost balance relations and the required auxiliary equations should be applied to each element of the system to determine the cost of exergy streams. For a system component the cost balance equation is defined as [45]:

$$\sum \dot{C}_{out,k} + \dot{C}_{w,k} = \sum \dot{C}_{in,k} + \dot{C}_{q,k} + \dot{Z}_{k,PY} \tag{48}$$

$$\dot{Z}_k = \dot{Z}_k^{CI} + \dot{Z}_k^{OM} \tag{49}$$

$$\dot{C} = c\dot{E} \tag{50}$$

$$\dot{C}_{out} = c_{out}\dot{E}_{out} \tag{51}$$

$$\dot{C}_q = c_q\dot{E}_q \tag{52}$$

$$\dot{C}_w = c_w\dot{E}_w \tag{53}$$

where $\dot{Z}_k^{OM}$ is the cost of operating and maintenance, c denotes specific exergy cost and $\dot{C}$ is the cost rate.

In addition, annual levelized capital investment for the kth component is defined [46]:

$$\dot{Z}_k^{CI} = \left(\frac{CRF}{\tau}\right)Z_k \tag{54}$$

where τ is annual plant operating hours which is assumed 8000 hr in this paper and *CRF* is capital recovery factor that can be determined as [47]:

$$CRF = \frac{i_r(1+i_r)^n}{(1+i_r)^n - 1} \tag{55}$$

The cost equations (Z_k) for every component of the system are tabulated in Table 2. Subsequently, Z_k for the present year ($Z_{k,PY}$, 2018) is calculated [48]:

$$Cost\ at\ present\ year = Original\ cost \times \frac{CEPCI\ of\ the\ present\ year}{CEPCI\ of\ the\ base\ year} \tag{56}$$

Here, i_r is the interest rate, and n is the number of operating years. Cost equations for the components of the proposed systems are tabulated in Table 2.

For determining the exergoeconomic parameters, cost rates of fuel $\dot{C}_F$ and product $\dot{C}_P$ are used as follow [50]:

$$c_{F,k} = \frac{\dot{C}_{F,k}}{\dot{E}_{F,k}} \tag{57}$$

$$c_{P,k} = \frac{\dot{C}_{P,k}}{\dot{E}_{P,k}} \tag{58}$$

$$\dot{C}_{D,k} = c_{F,k}\dot{E}_{D,k} \tag{59}$$

$$f_k = \frac{\dot{Z}_k}{\dot{Z}_k + \dot{C}_{D,k} + \dot{C}_{L,k}} \tag{60}$$

$$r_k = \frac{c_{P,k} - c_{F,k}}{c_{F,k}} \tag{61}$$

where $c_{F,k}$ is the unit cost of fuel, $c_{P,k}$ is the unit cost of the product, $\dot{C}_{D,k}$ is the cost rate of exergy destruction, f_k is the exergoeconomic factor, and r_k is the relative cost difference.

Cost balances for the components and auxiliary equations are tabulated in Table 3.

3.3. Performance examination

Energy efficiency of the integrated systems can be written as:

$$\eta_{I,a} = \frac{\dot{W}_{SOFC}}{\dot{m}_F LHV_F} \tag{62}$$

$$\eta_{I,b} = \frac{\dot{W}_{SOFC} + \dot{W}_{SE} - \dot{W}_P + \dot{Q}_{heating}}{\dot{m}_F LHV_F} \tag{63}$$

$$\eta_{I,c} = \frac{\dot{W}_{SOFC} + \dot{W}_{SE} - \dot{W}_P + \dot{Q}_{heating} - \dot{W}_{PEME} + \dot{m}_{H_2} LHV_{H_2}}{\dot{m}_F LHV_F} \tag{64}$$

where $\dot{Q}_{heating} = \dot{m}_{14}(h_{14} - h_{15})$ and $\eta_{I,a}$ $\eta_{I,b}$ *and* $\eta_{I,c}$ denote energy efficiency of the model (a), (b) and (c), respectively. $\dot{m}_F$ and LHV_F denote biomass (fuel) feeding rate and biomass lower heating value, respectively.

Additionally, exergy efficiencies of the proposed model (a), (b) and (c) are respectively defined as:

$$\eta_{II,a} = \frac{\dot{W}_{SOFC}}{\dot{E}_5} \tag{65}$$

$$\eta_{II,b} = \frac{\dot{W}_{SOFC} + \dot{W}_{SE} - \dot{W}_P + \dot{E}_{heating}}{\dot{E}_5} \tag{66}$$

$$\eta_{II,c} = \frac{\dot{W}_{SOFC} + \dot{W}_{SE} - \dot{W}_P + \dot{E}_{heating} - \dot{W}_{PEME} + \dot{E}_{18}}{\dot{E}_5} \tag{67}$$

Table 2
Cost equations for components of the proposed systems [10,13,49].

Component	Cost equations
Gasifier	$Z_G = 1600 \times (\dot{m}_{drybiomass})^{0.67}$
SOFC stack	$Z_{SOFC} = A_a N_{FC}(2.96T_{FC,e} - 1907)$
Afterburner	$Z_{AB} = \frac{46.08 \times \dot{m}_4}{(0.955 - (P_{11}/P_4))}(1 + e^{0.018T_{11} - 26.4})$
Air and fuel blowers	$Z_{AC} = Z_{AF} = 91562 \times \left(\frac{\dot{W}_{AC}}{455}\right)^{0.67}$
Circulation pump	$Z_P = 3 \times [442 \times (\dot{W}_P)^{0.71} \times 1.41 f_n]$
	$f_n = 1 + \frac{(1-0.8)}{(1-\eta_P)}$
AHX	$Z_{AHX} = 3 \times \left[130 \times \left(\frac{A_{AHX}}{0.093}\right)^{0.78}\right]$
Inverter	$Z_{inv} = 10^5 \times \left(\frac{\dot{W}_{SOFC,DC}}{500}\right)^{0.7}$
Stirling engine	$Z_{SE} = 2200 \times \dot{W}_{SE}$
PEME	$Z_{PEME} = 1000 \times \dot{W}_{PEME}$
$i_r = 0.12$, $n = 20$ years	

Table 3
Cost balances and auxiliary equations for the components.

Component	Cost balance	Auxiliary equations
Downdraft gasifier	$\dot{C}_5 + \dot{C}_6 + \dot{Z}_{G,PY} = \dot{C}_7$	$c_5 = 2$ \$/GJ $c_6 = 0$
Fuel blower	$\dot{C}_{W,FC} + \dot{C}_7 + \dot{Z}_{FC,PY} = \dot{C}_8$	$c_{W,FC} = c_{W,SOFC,AC}$
Air blower	$\dot{C}_{W,AC} + \dot{C}_1 + \dot{Z}_{AC,PY} = \dot{C}_2$	$c_1 = 0$ $c_{W,AC} = c_{W,SOFC,AC}$
Air heat exchanger	$\dot{C}_2 + \dot{C}_{11} + \dot{Z}_{AHX,PY} = \dot{C}_{12} + \dot{C}_{3a}$	$c_{11} = c_{12}$
Anode mixer	$\dot{C}_8 + \dot{C}_{9b} + \dot{Z}_{AM,PY}(0) = \dot{C}_9$	N/A
Cathode mixer	$\dot{C}_{3b} + \dot{C}_{3a} + \dot{Z}_{CM,PY}(0) = \dot{C}_3$	N/A
Stack	$\dot{C}_3 + \dot{C}_9 + \dot{Z}_{SOFC,stack,PY} = \dot{C}_4 + \dot{C}_{10} + \dot{C}_{W,SOFC,stack}$	$c_4 = c_{W,SOFC,DC}$ $c_{10} = c_{W,SOFC,DC}$
Inverter	$\dot{C}_{W,SOFC,DC} + \dot{Z}_{I,PY} = \dot{C}_{W,SOFC,AC}$	N/A
After burner	$\dot{C}_{10b} + \dot{C}_{4a} + \dot{Z}_{AB,PY} = \dot{C}_{11}$	$c_{10b} = c_{9b}$, $c_{4a} = c_{3b}$ $c_{10b} = c_{10}$, $c_{3b} = c_4$
Stirling engine	$\dot{C}_{12} + \dot{C}_{15} + \dot{Z}_{SE,PY} = \dot{C}_{14} + \dot{C}_{13} + \dot{C}_{W,SE}$	$c_{W,SE} = (c_{14}\dot{E}_{14} - c_{15}\dot{E}_{15})/(\dot{E}_{14} - \dot{E}_{15})$ $c_{12} = c_{13}$
Circulation pump	$\dot{C}_{W,P} + \dot{C}_{14} + \dot{Z}_{P,PY} = \dot{C}_{15}$	$c_{W,P} = c_{W,SE}$
PEME	$\dot{C}_{W,PEME} + \dot{Z}_{PEME,PY} = \dot{C}_{18}$	$c_{W,PEME} = c_{W,SE}$

where $\dot{E}_{55}$ is the total exergy of the inlet biomass fuel which can be calculated as described in the literature [7] and $\dot{E}_{heating} = \dot{E}_{14} - \dot{E}_{15}$.

Total specific product cost associated with the systems is defined as:

$$c_{p,tot} = \frac{\sum_{i=1}^{n_k} \dot{Z}_k + \sum_{i=1}^{n_F} \dot{C}_{Fi}}{\sum_{i=1}^{k} \dot{E}_{Pi}} \tag{68}$$

3.4. Environmental impact

Environmental impact of the proposed models is examined and compared by calculating the amount of CO_2 emitted from afterburner. For determining the normalized CO_2 emission of the model (a), (b) and (c), following equations are respectively used to estimate the amount of discharged CO_2 to the atmosphere:

$$\varepsilon_a = \frac{\dot{m}_{CO_2,emitted}}{\dot{W}_{SOFC}} \tag{69}$$

$$\varepsilon_b = \frac{\dot{m}_{CO_2,emitted}}{\dot{W}_{SOFC} + \dot{W}_{SE} - \dot{W}_P + \dot{E}_{heating}} \tag{70}$$

$$\varepsilon_c = \frac{\dot{m}_{CO_2,emitted}}{\dot{W}_{SOFC} + \dot{W}_{SE} - \dot{W}_P + \dot{E}_{heating} - \dot{W}_{PEME} + \dot{E}_{18}} \tag{71}$$

3.5. Multi-objective optimization

Facing various conflicting objectives in the thermal design systems is a usual problem that must be satisfied simultaneously. Commonly, installing a more efficient system costs higher than a less efficient one. Unlike single objective optimization, in an MOO, a set of the optimal solutions—namely Pareto frontier—is achieved. Finding an optimum point which is well-balanced between the system cost and efficiency is very important. Finding such spot is rather arduous since there may be a large number of practical design parameters in a system. On the other hand, designing a well-suited system can save colossal cost associated with the long-term operation of the plant and at the same time sustain acceptable performance. In such conditions, an MOO method based on genetic algorithm is a useful and feasible tool to determine the optimum design point and find the best values of the system design parameters. Thus in this study, an MOO method based on an evolutionary algorithm is implemented using a developed MATLAB code to assign the suitable design point.

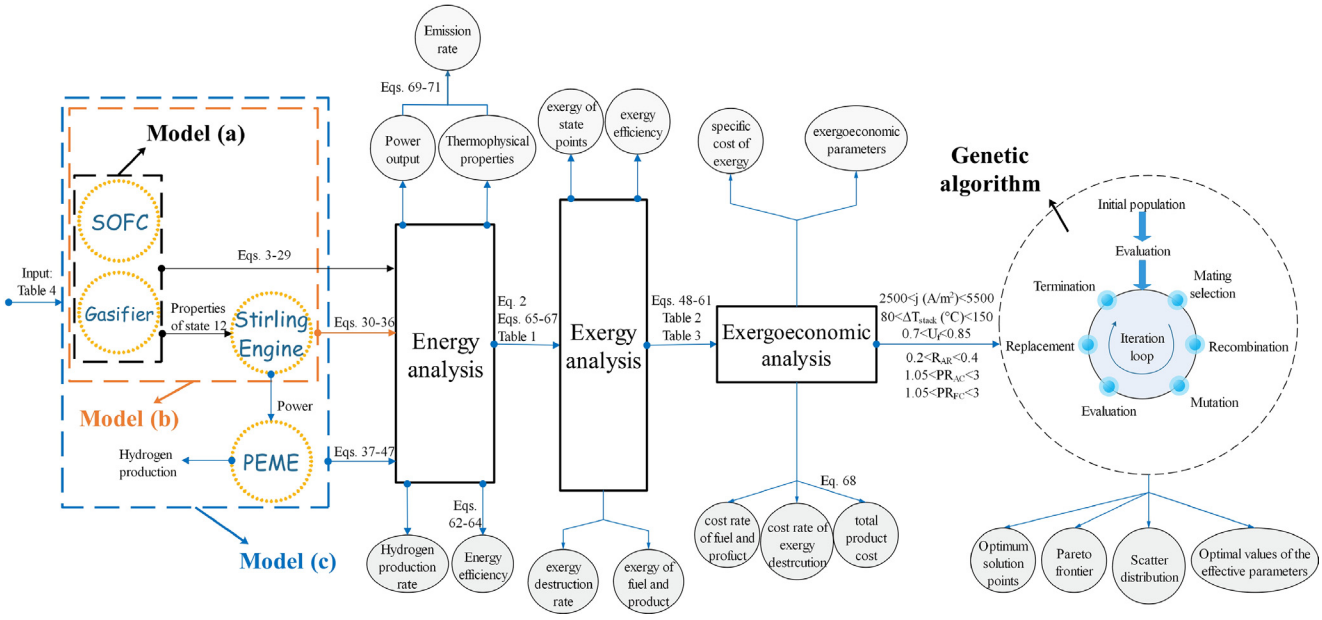

Fig. 2. Flowchart of modeling and optimization procedure of the proposed systems.

For the MOO, three conflicting objectives are considered in this study: exergy efficiency (Eqs. (65)-(67)) as a performance indicator (to be maximized), hydrogen production rate of the model (c) (to be maximized) and total product cost of the models (Eq. (68) as economic indicant (to be minimized)).

Modeling and optimization procedure of the proposed models are presented in Fig. 2.

4. Results and discussion

A parametric study is performed to examine the influence of main effective parameters on performance, economic and emission indicators. Furthermore, MOO of the proposed systems is investigated and Pareto frontier of the optimal solutions and scatter distribution of the effective parameters are presented.

4.1. Verification and validation

To validate the SOFC modeling reported experimental data by Tao et al. [51] is chosen and used to examine the influence of current density on the power density and cell voltage. Fig. 3(a) shows the results of this study along with the reported data by Tao et al. [51]; as shown in the figure, there is a good agreement between the results. Furthermore, to ensure the outcomes of modeling the PEME, cell potential results of the present model are compared to experimental results [52] and shown in Fig. 3(b) which shows a good agreement between the results. Moreover, modeling the SE of this study is compared to the numerical model of Hosseinpour et al. [16] as illustrated in Fig. 3(c). It can be seen that there is a decent agreement between the results. Eventually, to validate the gasification results of this study, syngas composition of the present model is compared to the numerical model [53], as shown in Fig. 3(d). Ash-free basis municipal solid waste is considered as feedstock at temperature of 1100 K. According to the figure, present results fit well on available numerical data.

Table 4
Input parameters for the SE, SOFC, gasifier, and PEME.

Parameter	Value	Parameter	Value
SOFC system		*Gasifier*	
j (A/m^2)	5000	Gasification temperature (°C)	600
U_f	0.85	Gasifier heat loss (%)	0
ΔT_{stack} (°C)	100	Biomass and air inlet temperature (°C)	25
R_{AR}	0.4	*PEME*	
R_{CR}	0.4	T_{PEME} (°C)	80
PR_{AC}	1.19	P_{O_2}, $P_{H_2}(kPa)$	101.3
PR_{FC}	1.19	$E_{act,a}$ (kJ/mol)	76
η_{inv}	0.97	$E_{act,c}$ (kJ/mol)	18
A_a (m^2)	0.01	λ_a	14
$T_{SOFC,inlet}$ (K)	1000	λ_c	10
j_{anode} (A/m^2)	6500	J_a^{ref} (A/m^2)	1.7×10^5
$j_{cathode}$ (A/m^2)	2500	J_c^{ref} (A/m^2)	4.6×10^3
Effective diffusivity of gases - anode (cm^2/s)	0.2	F (C/mol)	96,486
Effective diffusivity of gases - cathode (cm^2/s)	0.05	*Stirling Engine*	
Anode thickness (mm)	0.5	*RV*	1.23
Cathode thickness (mm)	0.05	$T_{heater,wall}$ (°C)	T_{12}
Electrolyte thickness (mm)	0.01	ΔT_{low} (°C)	60
Interconnect thickness (mm)	3	ΔT_{high} (°C)	100
Cell numbers	11,000	ΔT_{water} (°C)	40
Pressure drop through the stack (%)	2	$T_{water,inlet}$ (°C)	20
Pressure drop through the heat exchanger (%)	3	$\eta_{mech,SE}$	0.85
Pressure drop through the afterburner (%)	5	ε_{SE}	0.94
$\eta_{FC} = \eta_{AC}$	0.85	γ	1.667

4.2. Parametric study

In this section, the effect of major effective parameters is

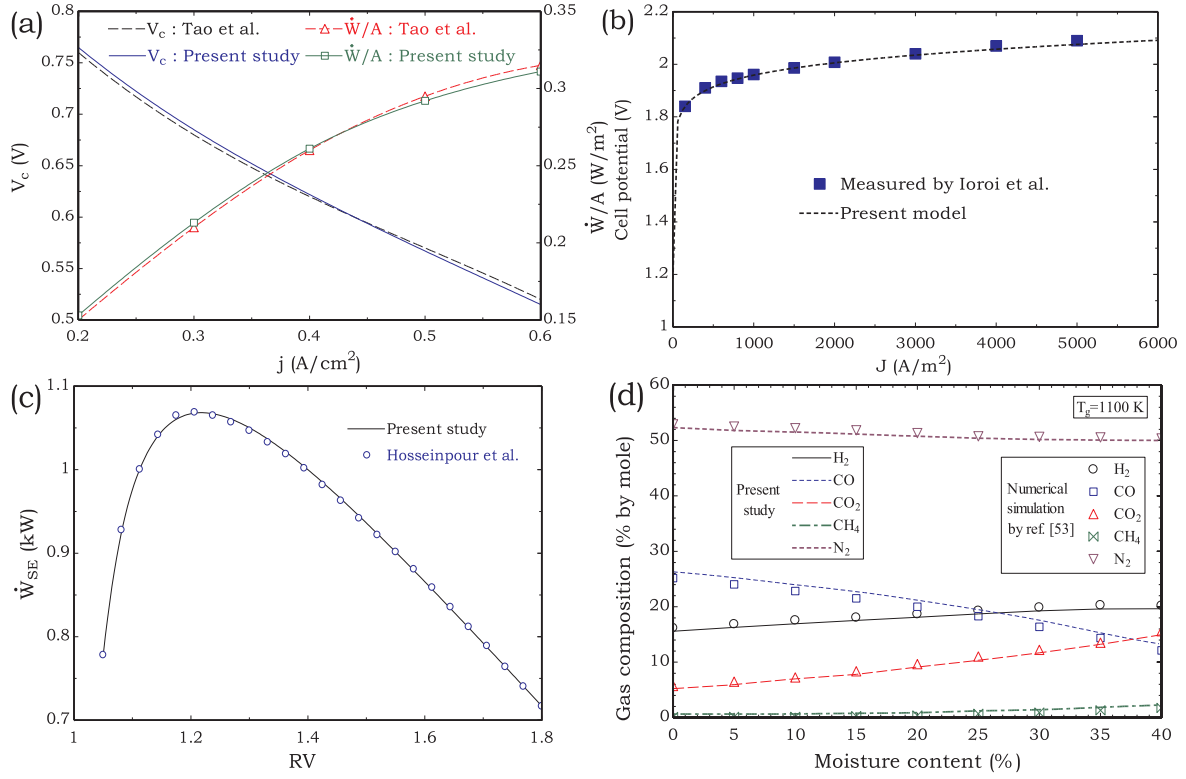

Fig. 3. (a) Validation of SOFC modeling, (b) validation of PEME modeling, (c) verification of SE modeling, (d) verification of gasifier modeling.

investigated on performance, economic and emission indicants in detail. Also, the input parameters as the base case are listed in Table 4.

The first active parameter is current density. By increasing the current density, the efficiency of all models will be expected to decrease. This can be explained because higher current density leads to higher H_2 consumption in the SOFC and thus increases the denominator of Eqs. (65)–(67). As shown in Fig. 4(a), by altering the current density from 2000 A/m^2 to 5500 A/m^2, exergetic efficiency of the models fall while the exergy efficiency of the model (b) and (c) remains higher than the effectiveness of the first model. Additionally, the costs associated with the systems decrease at the beginning until the costs become minimum and after that rises by increasing the current density. Such trends in the price and exergetic efficiency show the importance of MOO. The net power output of the systems is observed in Fig. 4(b) to increase as the current density rises while the energy efficiencies decrease. Increasing the power is justified because rising the current density will overcome the cell voltage diminution which would increase the power output. The net power output of the second model increases at a faster rate than the other models (because SE power grows at a more rapid rate). The power output of the model (a) and (c) are equal since the power of SE is used in PEME. The rate of hydrogen production also increases in the reasonable range of current density since the power output of the SE rises, and this means higher available power for PEME for hydrogen production. The figure reveals that the model (b) is the best-proposed model.

As illustrated in Fig. 5(a), by increasing stack temperature difference from 80 °C to 150 °C, total product costs of the systems decrease while the exergy efficiencies increase. It can be seen that total product cost of the model (a) declines at a faster rate. Also as shown in Fig. 5(b), by increasing the temperature difference in the mentioned range, the power output and energy efficiency of the models increase. Such increase is because the inlet temperature of the SOFC is fixed, increasing stack temperature difference means rising the outlet enthalpy, which results in a clear increase in the power output of the models. Additionally, the rate of hydrogen production increases by raising the temperature difference since the available power for PEME increases.

Fig. 6 shows the effect of utilization factor on the performance of the systems. As displayed in the figure, by increasing utilization factor from 0.7 to 0.85, total product costs initially decrease therafter rise in all models. The trend of exergy efficiency is on the contrary of the costs trends since it grows at first then drops. As shown in Fig. 6(b) the energy efficiencies reduce by increasing the utilization factor. The figure further indicates that power output of the first and third model has a maximum point while the power output of the model (b) continually decreases. Since the SE power output (which is used in PEME) decreases by raising the utilization factor, the rate of hydrogen production decreases.

Influence of the anode recycling ratio (R_{AR}) is examined on the performance of the models in Fig. 7. As the figure shows, the total product costs decrease where they reach the corresponding minimum value while the exergy efficiencies increase to achieve the highest values. Similar trends can be seen from energy efficiency and net power output viewpoints. The figure further shows by increasing the anode recycling ratio; the SE power output decreases since the enthalpy of the off-gases decreases which leads to a reduction in hydrogen production rate.

Effect of cathode recycling ratio is also investigated which is depicted in Fig. 8. As the figure indicates, by raising the cathode recycling ratio, energy, and exergy efficiencies together with net power outputs increase. Total product costs would be decreased by increasing the proportion. Contrary to anode recycling ratio, by increasing the cathode recycling ratio, the SE power output increases (this is because the enthalpy of the exhaust gases rises) so the available power for hydrogen production increases, hence higher hydrogen production rate is expected.

The pressure ratio of air blower can affect the performance of the system as the Fig. 9 shows. The figure reveals that, by increasing the pressure ratio from 1.05 to 3, Exergy efficiencies and net power output of the models decrease. By increasing the ratio, energy efficiency of the model (b) slightly increases while the energy efficiency of the model (c) slightly decreases. Energy efficiency of the model (a) falls too but at a faster rate. Additionally, it can be seen that raising the pressure ratio will increase the SE power output which leads to higher hydrogen production in the model (c). Total product costs associated with the models increase by raising the pressure ratio where the total cost of the first model rises at a very faster rate than other models.

Fig. 10 reveals the effect of the fuel blower pressure ratio on the system performance. The inference from the figure is that raising the pressure ratio will increase the energy and exergy efficiencies and net power output while the total production costs would decrease. The pressure ratio cannot be such effective on SE power output, which leads to a relatively constant hydrogen production rate. Further increase of the pressure ratio to higher than 2, may not affect the system performance by much.

Another chosen parameter is ζ, which denotes the lowest over the highest temperature of the Stirling cycle. As depicted in Fig. 11, by increasing ζ, the Stirling polytropic efficiency (η_{pcy}) decreases, so the power generation of the SE will decrease (Eqs. (30) and (32)). Also, the increment of ζ decreases exergetic efficiency of models (b) and (c) and hydrogen production rate (Eqs. (66) and (67)). The SE power output will not affect upper cycle, so the performance and economic indicators of the model (a) remain constant. By increasing the ζ, total product cost of the model (b) increases while total product cost associated with the model (c) decreases. Moreover, it can be seen that by increasing the ζ, energy efficiency of the model (b) remains constant while the efficiency of the model (c) slightly increases.

Effect of piston compression ratio in SE (RV) is also examined as illustrated in Fig. 12. Similar to ζ, RV cannot be useful on the

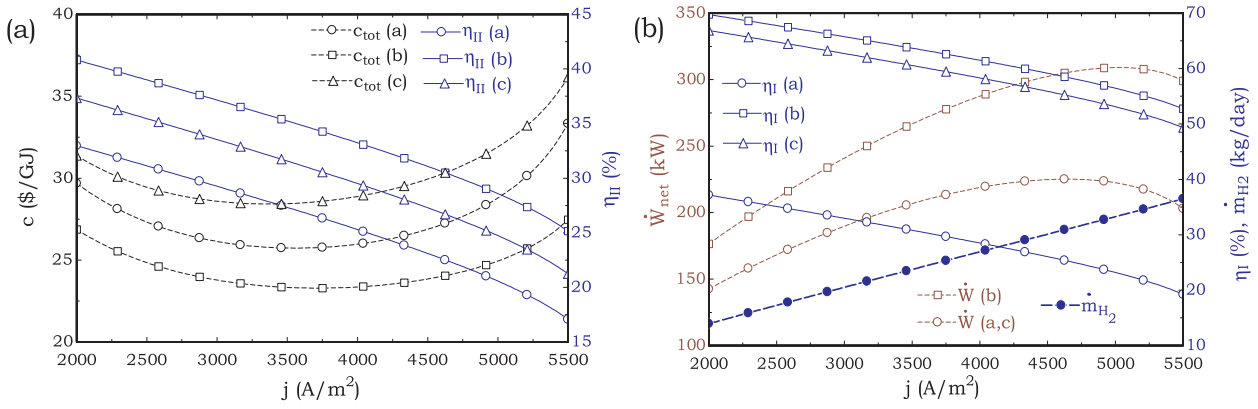

Fig. 4. Influence of current density on total cost, exergetic efficiency, energy efficiency, power output and rate of hydrogen production of the proposed systems.

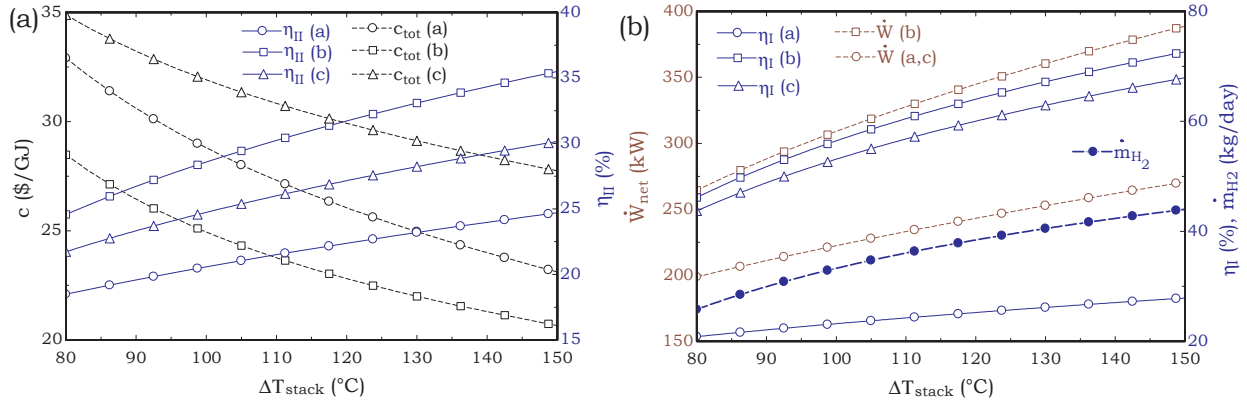

Fig. 5. Effect of the stack temperature difference on the total cost, exergetic efficiency, energy efficiency, power output and rate of hydrogen production of the proposed systems.

performance of the first model. Also, by increasing *RV*, the energy efficiency of the model (b) does not change while the effectiveness of the third model initially decreases and after that increases. As the figure further reveals, there is a maximum point in the aspect of exergy efficiencies, net power output, and rate of hydrogen production. $RV \sim 1.2$ would be an optimum ratio because all the performance indicators (except total product cost of the third model) would reach their optimum values. Despite, at $RV \sim 1.2$ total product cost associated with the third model is the highest value, but it is acceptable since the difference between the lowest and highest price is not considerable.

4.3. Environmental impact

The amount of CO_2 emitted to the atmosphere of the proposed systems is compared by implementing Eqs. (69)–(71). As the Fig. 13 shows, model (b) has the lowest amount of emission indicator among the proposed systems and model (c) has lower levelized emission compared to model (a).

Results of the parametric study and environmental impact reveal that model (b) is the most suitable model in the aspect of energy, exergy, exergoeconomic and environmental viewpoints. Model (c) has some benefits over the model (a): higher energy and exergy efficiency, lower emission indicant and capability of hydrogen production. Additionally, higher total product cost can be assumed as the main disadvantage of the model (c) compared to model (a) and (b). Eventually, it can be concluded that if exergy efficiency and total product cost/lower emission is considered, model (b) would be the most suitable system. If hydrogen production is needed and at the same time exergy efficiency and environmental pollution would be maintained at an acceptable range, model (c) may be a better system.

4.4. Thermodynamic properties, exergy, and exergoeconomic analysis

Thermodynamic parameters together with cost and cost rate of each stream of the proposed models are tabulated in Table 5.

Exergy of fuel and products, exergy destruction additionally exergoeconomic parameters are summarized in Table 6. The higher values for exergoeconomic factor reveal that the purchase cost of the equipment is high. Thus, the high amount of *f* for the stack shows that reducing the capital investment cost would be cost-effective at such material. The low amount of exergoeconomic factor (such as AHX) is equivalent to the higher value of $\dot{Z}_k + \dot{C}_D$, which is the result of higher exergy destruction costs and more irreversibility.

4.5. Multi-objective optimization

Six major effective parameters for each model is considered to perform MOO on the systems. The parameters and their reasonable ranges are listed in Table 7.

Using genetic algorithm the optimal solution points of the integrated systems are illustrated in Fig. 14, as Pareto frontiers. Total product cost, exergy efficiency, and hydrogen production rate are considered as the objective functions. As the figure shows, total product cost of the integrated systems increases by increasing exergy efficiency. From point C to A, the exergy efficiency rises and overall cost increases in all models. Additionally, for the model (c), the rate of hydrogen production and overall product cost increase. Indeed, point A is the optimum point in the aspect of exergy efficiency/hydrogen production rate and point C is the optimum one when total cost is important. The ideal operating point of the proposed systems is shown in the figure as it indicates the highest exergy efficiency/hydrogen production rate and

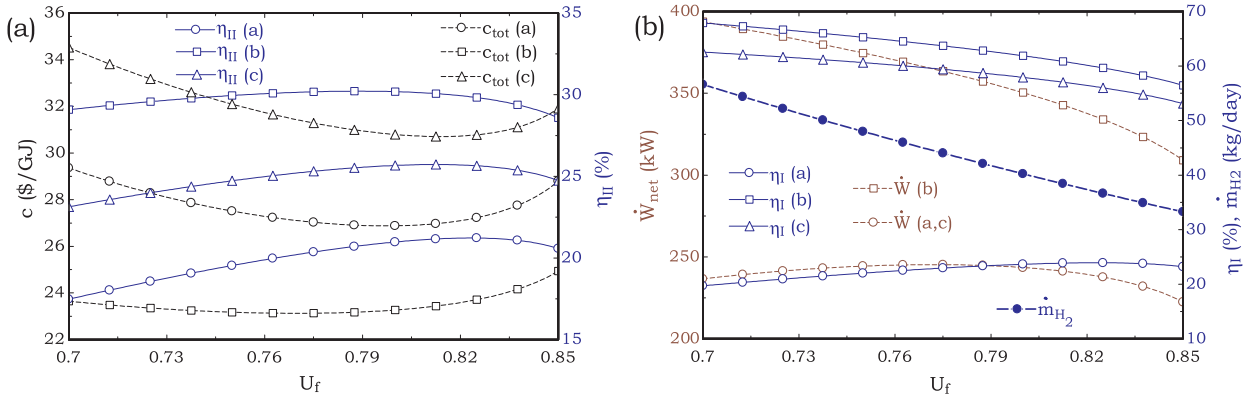

Fig. 6. Effect of utilization factor on the total product cost, exergetic efficiency, energy efficiency, power output and rate of hydrogen production of the proposed systems.

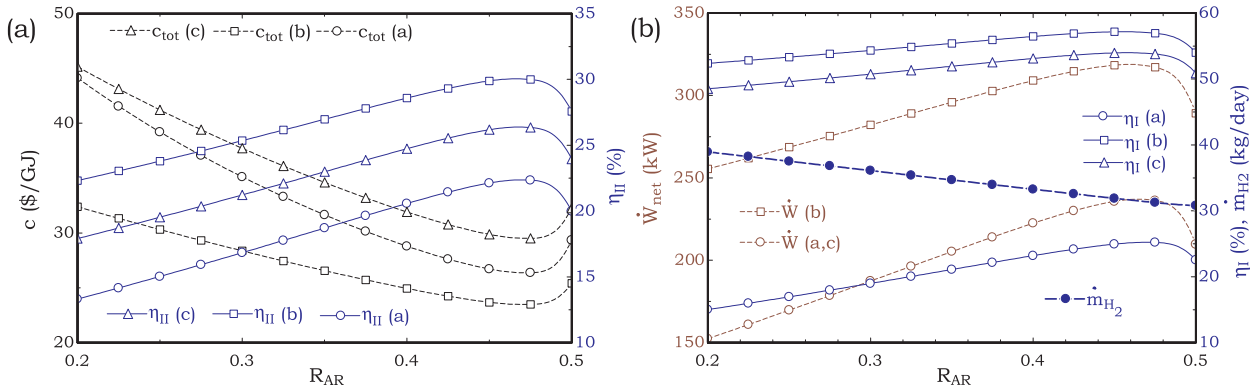

Fig. 7. Effect of recycling anode ratio on total product cost, exergetic efficiency, energy efficiency, power output and rate of hydrogen production of the proposed systems.

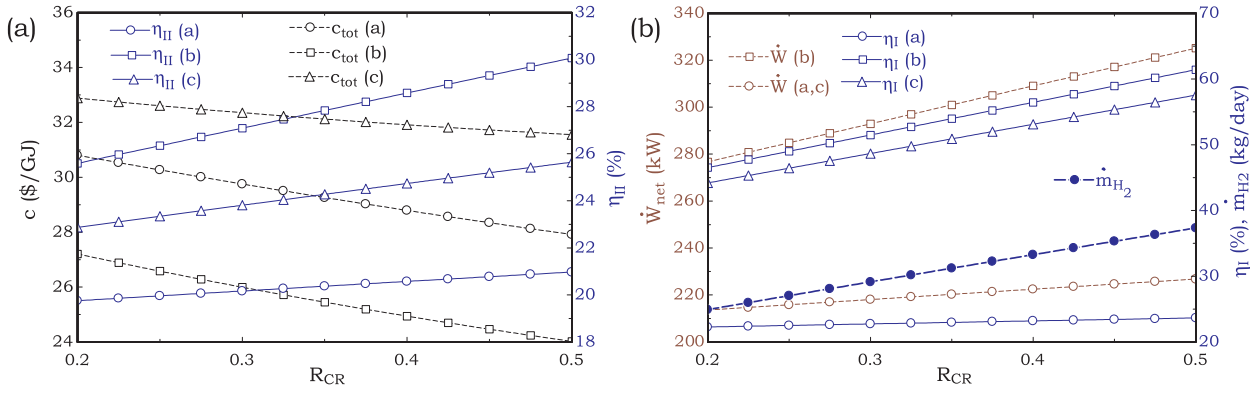

Fig. 8. Effect of the recycle cathode ratio on total product cost, exergetic efficiency, energy efficiency, power output and rate of hydrogen production of the proposed systems.

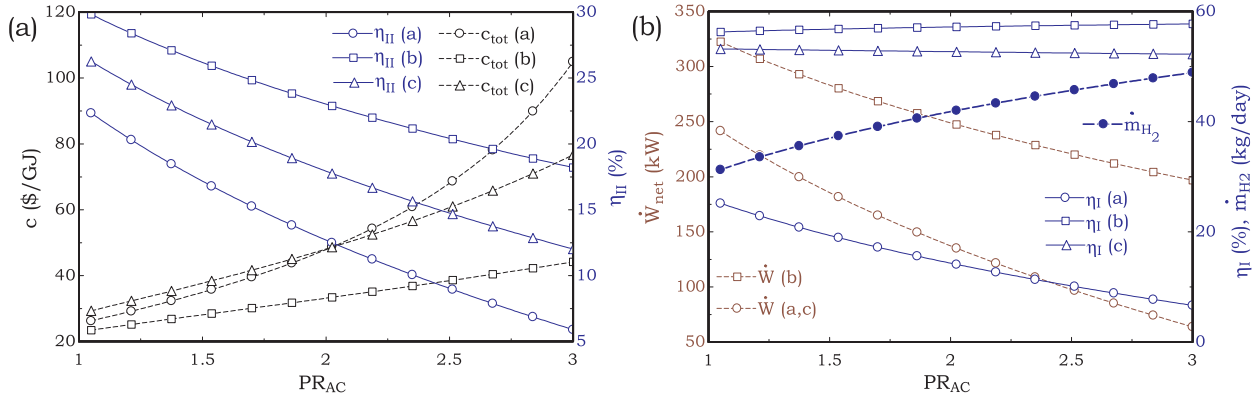

Fig. 9. Effect of air blower pressure ratio on total product cost, exergetic efficiency, energy efficiency, power output and rate of hydrogen production of the proposed systems.

the lowest total product cost. Obviously, reaching this point is impossible; hence, the two objective functions never conclude their highest optimum value at the same time. Therefore, the closest point to the ideal position, which is located on the Pareto frontiers, is chosen as the best final solution since the systems are well-balanced at this point (point B).

The values of the chosen effective parameters and emission indicator on points A, B, and C are tabulated in Table 8.

To have a better overview of the influence of the variation of the effective parameters, scatter distributions of the effective parameters are investigated. The results indicate that, in the model (a), R_{AR} and PR_{FC} should be kept at their highest values where all the optimal solutions are located. PR_{AC}, on the other hand, should be held at its lowest value. The range of ΔT_{stack}, j, and U_f around of 130–135 °C, 4500–4800 A/m^2 and 0.8–0.85 is preferred since these ranges cover all the optimum solution points.

Scatter distribution of the optimal solutions of the model (b) which is shown in Fig. 15 reveals that for R_{AR}, ΔT_{stack}, and PR_{FC} the highest values are favorable. The most suitable ranges of the other effective parameters are: $2500 < j$ (A/m^2) < 5100, $0.75 < U_f < 0.85$, $1.05 < PR_{AC} < 1.8$.

If exergy efficiency and total product cost are assumed to be the objective functions for the model (c), highest values of R_{AR} and U_f may be a better design choice. Also, keeping the ΔT_{stack} and PR_{AC} close to 148 °C and 1.05 would be favorable. Also, j between 2800 A/m^2 and 3800 A/m^2, PR_{FC} between 1.9 and 2.5 are preferred where all the

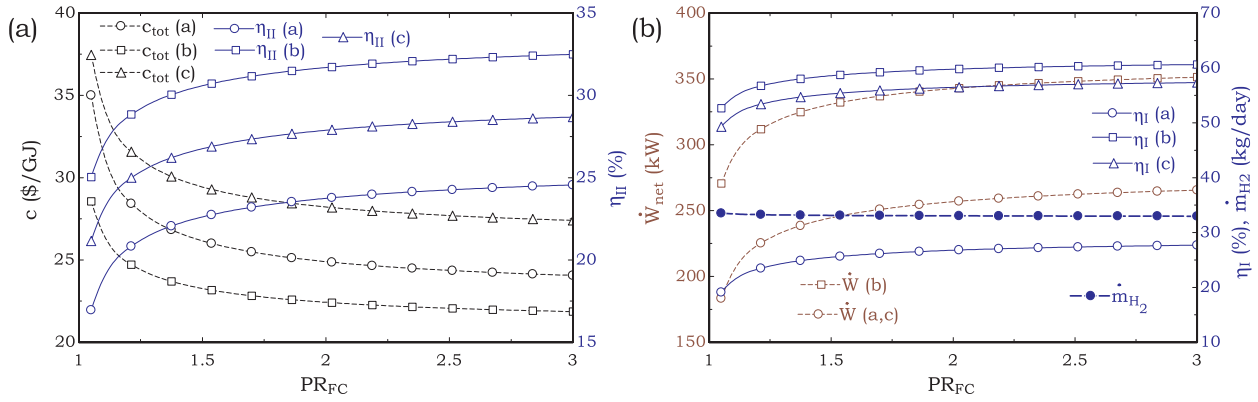

Fig. 10. Effect of fuel blower pressure ratio on total product cost, exergetic efficiency, energy efficiency, power output and rate of hydrogen production of the proposed systems.

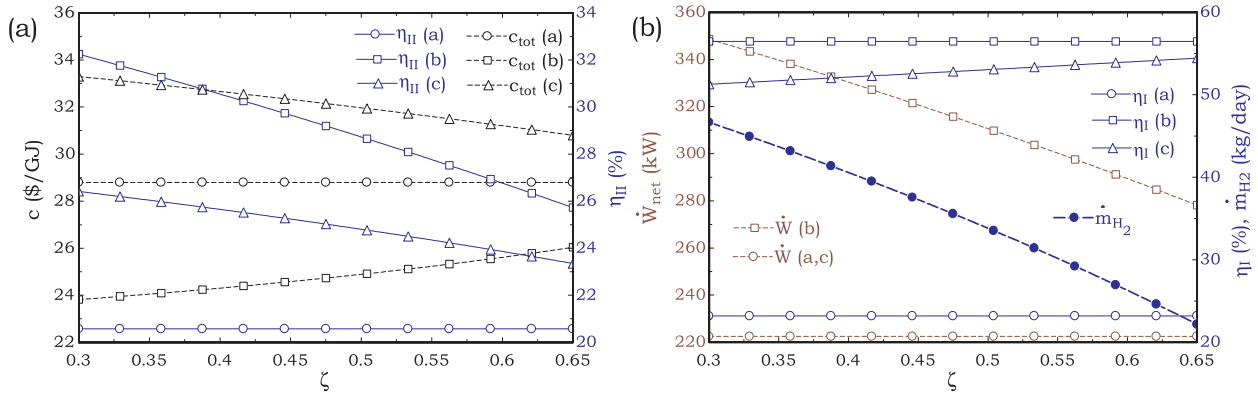

Fig. 11. Effect of ζ on total product cost, exergetic efficiency, energy efficiency, power output and rate of hydrogen production of the proposed systems.

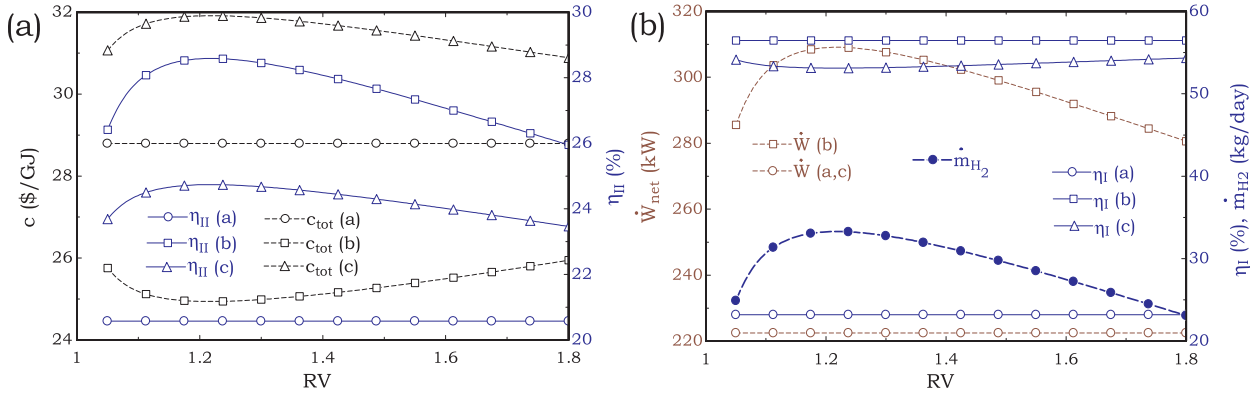

Fig. 12. Effect of RV on total product cost, exergetic efficiency, energy efficiency, power output and rate of hydrogen production of the proposed systems.

optimal solution points are located.

If $\dot{m}_{H_2}$and $c_{p,tot}$ are considered as the objective functions for the model (c), the highest values of ΔT_{stack}, the lowest values of U_f and $j \sim 5400$ A/m^2 are recommended. Moreover, further evaluation of scatter distribution reveals that optimum solution points of R_{AR}, $PR_{FC,}$ and PR_{AC} are dispersed on the whole range albeit lower values of PR_{FC} are favorable.

Eventually, performance and economic indicators of the proposed integrated systems are compared to the literature with similar concept of the present study. The proposed concepts of this study represent a biomass based anode/cathode recycling SOFC along with two novel concepts including Stirling engine and PEM electrolyzer. On the other hand, the proposed model of Sadeghi et al. [28] consists of a conventional biomass based anode recycling SOFC. In both researches, the equilibrium model has been implemented to simulate the gasification process with MSW as the feedstock. Furthermore, Sadeghi et al. [28] optimized the system by MOO method implementing the genetic algorithm. Side by side comparison of the performance and economic indicants on the best optimized solution point is provided in Table 9. Higher exergy efficiency in all proposed models and lower total product cost of models (a) and (b) are achieved by the new concepts of this study. Cathode recycling can increase the exergy efficiency as the comparison of the model (a) to the proposed model by Sadeghi et al. [28], indicates.

5. Conclusion

In the present work, three models based on gasification and SOFC are proposed: model (a): biomass gasifier is integrated with SOFC, model (b): off-gases of the first model is exploited in an SE to enhance

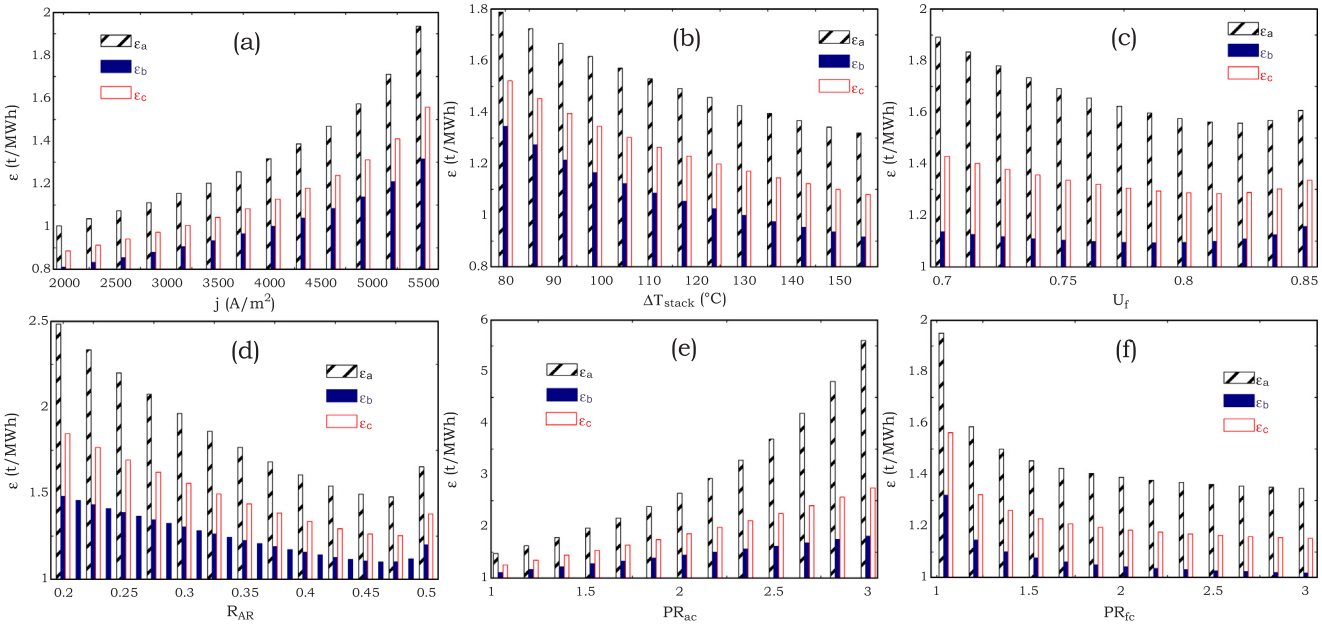

Fig. 13. The amount of CO_2 emission of the proposed systems by varying effective parameters.

Table 5
Thermodynamic parameters, cost and cost rate of each stream point of the proposed systems.

State	T (°C)	P (kPa)	$\dot{n}$ (kmol/s)	$\dot{E}$ (kW)	c ($/GJ)	$\dot{C}$ ($/h)	Molar fraction (%)						
							CH_4	H_2	H_2O	CO	CO_2	O_2	N_2
1	25	101.3	52.09	6.69	0	0	0	0	0	0	0	21	79
2	43.95	120.6	52.09	29.99	19.92	2.15	0	0	0	0	0	21	79
3a	661.2	118.2	52.09	471.6	21.56	26.60	0	0	0	0	0	21	79
3b	826.9	113.5	33.78	487.3	12.99	22.78	0	0	0	0	0	18.78	81.22
3	726.9	115.8	85.87	958	17.22	59.38	0	0	0	0	0	20.13	79.87
4a	826.9	113.5	50.67	683.1	12.99	31.93	0	0	0	0	0	18.78	81.22
4	826.9	113.5	84.44	1139	12.99	53.22	0	0	0	0	0	18.78	81.22
5	25	101.3	2.82	1081	2	7.79	–	–	–	–	–	–	–
6	25	101.3	3.35	0	0	0	0	0	0	0	0	21	79
7	600	101.3	6.47	847.7	3.264	9.96	5.35	17.32	6.41	14.89	14.66	0	41.39
8	646.4	120.5	6.47	883.1	4.73	15.03	5.35	17.32	6.41	14.89	14.66	0	41.39
9	726.9	120.5	11.24	1073	6.38	24.62	3.06	11.76	15.09	10.41	19.98	0	39.69
9b	826.9	118.1	4.77	205.1	12.99	9.59	0	4.21	26.86	4.33	27.19	0	37.40
10	826.9	118.1	7.47	526.6	12.99	24.62	0	6.73	42.91	6.92	43.44	0	59.75
10b	826.9	118.1	7.16	307.7	12.99	14.38	0	4.22	26.86	4.33	27.19	0	37.40
11	907.8	107.9	57.52	930.3	14.09	47.20	0	0	3.87	0	3.92	16.01	76.20
12	397.2	105.7	57.52	265.2	14.09	13.46	0	0	3.87	0	3.92	16.01	76.20
13	120	101.3	57.52	48.23	14.09	2.45	0	0	3.87	0	3.92	16.01	76.20
14	60	101.3	0.08	11.06	37.42	1.49	0	0	100	0	0	0	0
15	20	91.2	0.08	0.25	74.98	0.06	0	0	100	0	0	0	0
18	80	101.3	1.91e-4	45.01	88.74	14.38	0	100	0	0	0	0	0

$c_{W,SE} = c_{W,PEME} = c_{W,P}$ = 36.57 $/GJ, $c_{W,SOFC,AC}$ = 15.76 $/GJ

Table 6
Results of exergy and exergoeconomic analyses.

Component	$\dot{E}_F$ (kW)	$\dot{E}_P$ (kW)	$\dot{E}_D$ (kW)	η_{II} (%)	c_F ($/GJ)	c_P ($/GJ)	$\dot{C}_D$ ($/h)	$\dot{C}_L$ ($/h)	$\dot{Z}$ ($/h)	f (%)	r (%)
Downdraft gasifier	1081	847.7	233.3	78.41	2	3.264	1.7	0	2.177	56.14	63.2
Fuel blower	72.34	35.36	36.98	48.89	15.76	60.45	2.098	0	0.965	31.51	283.5
Air blower	28.74	23.3	5.44	81.06	15.76	25.65	1.631	0	0.520	62.73	62.7
Air heat exchanger	665.2	441.7	223.5	66.4	14.09	21.67	11.34	11.34	0.701	3	53.7
Anode mixer	1088	1073	15	98.56	6.284	6.376	0.731	0	0	0	1.5
Cathode mixer	959	958.05	0.95	99.9	17.2	17.22	0.044	0	0	0	0.098
Stack	2030.9	1999	31.9	98.43	11.49	12.99	1.321	0	9.43	87.72	13
After burner	990.8	930.3	60.5	93.9	12.99	14.09	2.825	0	0.889	23.94	8.5
Inverter	333.5	323.5	10	97	12.99	15.76	0.468	0	2.768	85.55	21.4
Stirling engine	160.3	97.42	62.92	60.76	14.09	36.57	3.193	5.32	4.689	59.49	159.4
Pump	0.015	0.015	0	100	36.56	74.98	0	0	0.002	100	105.1
PEME	86.61	45.01	41.6	51.97	36.57	88.74	5.476	0	2.979	35.24	142.7
Hydrogen production rate: 33.27 kg/day											

Table 7
Major effective parameters, which are used in the MOO and their reasonable ranges.

Parameter	Range
Current density (j, A/m^2)	$2500 < j < 5500$
Stack temperature difference (ΔT_{stack}, °C)	$80 < \Delta T_{stack} < 150$
Utilization factor (U_f)	$0.7 < U_f < 0.85$
Anode recycling ratio (R_{AR})	$0.2 < R_{AR} < 0.4$
Air blower pressure ratio (PR_{AC})	$1.05 < PR_{AC} < 3$
Fuel blower pressure ratio (PR_{FC})	$1.05 < PR_{FC} < 3$

the power/efficiency and model (c): surplus power of model (b) which is generated by SE is transfered into a PEME for hydrogen production. The proposed models are assessed from energy, exergy, exergoeconomic and environmental impact standpoints. A parametric study is performed to examine the influence of the major effective parameters on performance indicants and also the amount of levelized CO_2 emission. Additionally, exergoeconomic parameters together with exergy destruction of the components are calculated. Accordingly, the proposed models are optimized by MOO method to determine the best optimal solution point, which is well-balanced between the objective functions. Eventually, scatter distribution of the effective parameters is investigated to ascertain the best optimum operating ranges. Main conclusions of this study may be summarized as:

- The parametric study indicates that model (b) has the highest exergy efficiency at the same time lowest total product cost compared to model (a) and (c).
- Model (c) would be a more suitable model compared to model (a) because of higher exergy efficiency and hydrogen production capability.
- The thermodynamic and thermoeconomic analysis reveals that gasifier has the highest exergy destruction and stack and pump have the highest exergoeconomic factors.
- In optimum solution points, exergy efficiency of the model (a), (b), and (c) would be 28.51%, 39.41%, and 38.03%, respectively.
- Total product cost of the systems at the optimal operating condition may be 19.33 $/GJ, 18.91 $/GJ and 24.93 $/GJ respectively for models (a), (b) and (c).
- If the rate of hydrogen production and total product cost of the third model considered as the objective functions, the corresponding values at the best solution point are 56.5 kg/day and 41.76 $/GJ.
- Scatter distribution of the effective parameters indicates that anode

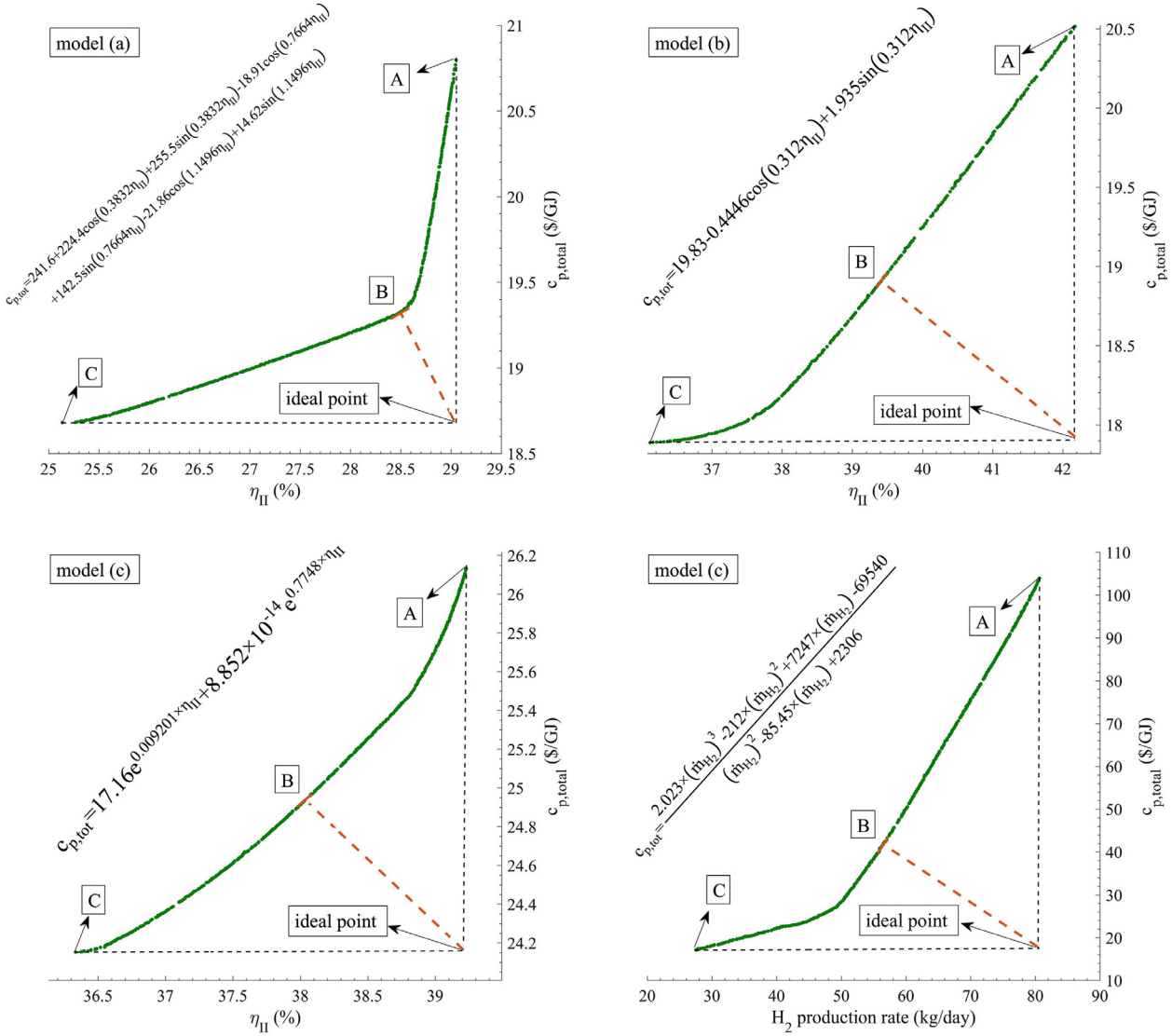

Fig. 14. The Pareto frontiers of the proposed models as optimal solutions for total product cost and exergy efficiency/hydrogen production rate as objective functions.

Table 8
MOO results on Points A, B, and C for the proposed systems.

Point	j (A/m^2)	ΔT_{stack} (°C)	U_f	R_{AR}	PR_{AC}	PR_{FC}	η_I (%)	η_{II} (%)	$c_{p,tot}$ ($/GJ)	$\dot{m}_{18}$ (kg/day)	ε (t/MWh)
Model (a)											
A	4698	134	0.844	0.4	1.052	2.99	31.67	29.05	20.80	–	1.119
B	4760	129	0.837	0.4	1.051	3.00	31.13	28.51	19.33	–	1.147
C	4766	130	0.811	0.4	1.050	2.99	28.22	25.44	18.68	–	1.180
Model (b)											
A	3311	150	0.848	0.4	1.267	2.99	69.91	42.15	20.51	–	0.5205
B	4563	150	0.844	0.4	1.440	3.00	67.38	39.41	18.91	–	0.7113
C	5072	150	0.749	0.4	1.760	3.00	64.21	36.12	17.89	–	0.8983
Model (c): η_{II} and $c_{p,tot}$ as the objective functions											
A	2851	148	0.85	0.4	1.05	1.57	67.72	39.23	26.13	24.15	0.8557
B	3124	148	0.85	0.4	1.05	1.93	66.41	38.03	24.93	26.30	0.7694
C	3737	148	0.85	0.4	1.05	2.00	64.54	36.33	24.15	31.29	0.8020
Model (c): H_2 production rate and $c_{p,tot}$ as the objective functions											
A	5432	148	0.70	0.2	2.00	1.20	37.23	8.85	103.90	80.66	3.737
B	5431	149	0.70	0.4	2.29	1.22	54.78	26.51	41.76	56.50	1.182
C	3138	150	0.70	0.4	1.172	2.96	57.10	28.72	17.10	27.54	0.601

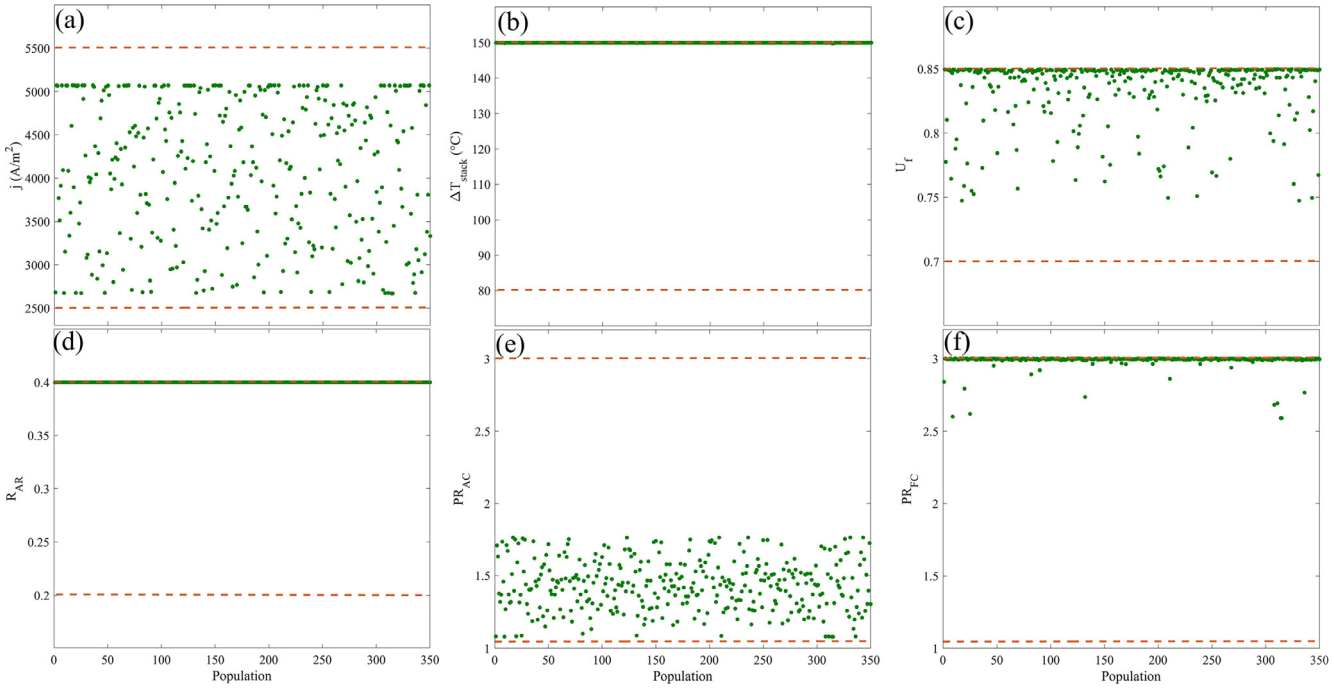

Fig. 15. Scatter distribution of the effective parameters of the model (b).

Table 9
Side by side comparison of exergy efficiency, total product cost, and rate of hydrogen production of the proposed models of this study with the literature on Point B.

Concept	Exergy efficiency (%)	Total product cost ($/GJ)	Hydrogen production (kg/day)
Biomass based anode recycling SOFC by Sadeghi et al. [28]	18.2	20.12	–
Biomass based anode/cathode recycling SOFC (model (a) of present study)	28.51	19.33	–
Biomass based anode/cathode recycling SOFC integrated with Stirling engine (model (b) of the present study)	39.41	18.91	–
Biomass based anode/cathode recycling SOFC integrated with Stirling engine and PEME (model (c) of the present study-exergy efficiency and total product cost considered as the objective functions)	38.03	24.93	26.30
Biomass based anode/cathode recycling SOFC integrated with Stirling engine and PEME (model (c) of the present study-hydrogen production rate and total product cost considered as the objective functions)	26.51	41.76	56.50

recycling ratio is the most sensitive parameter in all models.

Acknowledgment

The present study is carried out at the School of Mechanical Engineering, College of Engineering, University of Tehran. Consequently, we would like to express our sincere thanks and appreciation to the members of the Bioenergy Laboratory, who have made helpful suggestions in the preparation of this work and for their general support.

References

[1] Gholamian E, Zare V. A comparative thermodynamic investigation with environmental analysis of SOFC waste heat to power conversion employing Kalina and Organic Rankine Cycles. Energy Convers Manag 2016;117. http://dx.doi.org/10.1016/j.enconman.2016.03.011.
[2] Shijaz H, Attada Y, Patnaikuni VS, Vooradi R, Anne SB. Analysis of integrated gasification combined cycle power plant incorporating chemical looping combustion for environment-friendly utilization of Indian coal. Energy Convers Manag 2017;151:414–25. http://dx.doi.org/10.1016/j.enconman.2017.08.075.
[3] Zhang X, Chan SH, Li G, Ho HK, Li J, Feng Z. A review of integration strategies for solid oxide fuel cells. J Power Sources 2010;195:685–702. http://dx.doi.org/10.1016/j.jpowsour.2009.07.045.
[4] Ghaffarpour Z, Mahmoudi M, Mosaffa AH, Garousi Farshi L. Thermoeconomic assessment of a novel integrated biomass based power generation system including gas turbine cycle, solid oxide fuel cell and Rankine cycle. Energy Convers Manag 2018;161:1–12. http://dx.doi.org/10.1016/j.enconman.2018.01.071.
[5] De Lorenzo G, Fragiacomo P. Energy analysis of an SOFC system fed by syngas. Energy Convers Manag 2015;93:175–86. http://dx.doi.org/10.1016/j.enconman.2014.12.086.
[6] Speidel M, Kraaij G, Wörner A. A new process concept for highly efficient conversion of sewage sludge by combined fermentation and gasification and power generation in a hybrid system consisting of a SOFC and a gas turbine. Energy Convers Manag 2015;98:259–67. http://dx.doi.org/10.1016/j.enconman.2015.03.101.
[7] Gholamian E, Zare V, Mousavi SM. Integration of biomass gasification with a solid oxide fuel cell in a combined cooling, heating and power system: a thermodynamic and environmental analysis. Int J Hydrogen Energy 2016;41:20396–406.
[8] Mortazaei M, Rahimi M. A comparison between two methods of generating power, heat and refrigeration via biomass based solid oxide fuel cell: a thermodynamic and environmental analysis. Energy Convers Manag 2016;126:132–41. http://dx.doi.org/10.1016/j.enconman.2016.07.074.
[9] Tan L, Dong X, Gong Z, Wang M. Investigation on performance of an integrated SOFC-GE-KC power generation system using gaseous fuel from biomass gasification. Renew Energy 2017;107:448–61. http://dx.doi.org/10.1016/j.renene.2017.02.012.
[10] Sánchez D, Chacartegui R, Torres M, Sánchez T. Stirling based fuel cell hybrid systems : an alternative for molten carbonate fuel cells. J Power Sources 2009;192:84–93. http://dx.doi.org/10.1016/j.jpowsour.2008.12.061.
[11] Rokni M. Thermodynamic analyses of municipal solid waste gasification plant integrated with solid oxide fuel cell and Stirling hybrid system. Int J Hydrogen Energy 2015;40:7855–69. http://dx.doi.org/10.1016/j.ijhydene.2014.11.046.
[12] Entezari A, Manizadeh A, Ahmadi R. Energetical, exergetical and economical optimization analysis of combined power generation system of gas turbine and Stirling engine. Energy Convers Manag 2018;159:189–203. http://dx.doi.org/10.1016/j.enconman.2018.01.012.
[13] Rokni M. Thermodynamic and thermoeconomic analysis of a system with biomass gasification, solid oxide fuel cell (SOFC) and Stirling engine. Energy 2014;76:19–31. http://dx.doi.org/10.1016/j.energy.2014.01.106.
[14] Sowale A, Kolios AJ, Fidalgo B, Somorin T, Parker A, Williams L, et al. Thermodynamic analysis of a gamma type Stirling engine in an energy recovery system. Energy Convers Manag 2018;165:528–40. http://dx.doi.org/10.1016/j.enconman.2018.03.085.
[15] Ranjbar F, Chitsaz A, Mahmoudi SMS, Khalilarya S, Rosen MA. Energy and exergy assessments of a novel trigeneration system based on a solid oxide fuel cell. Energy Convers Manag 2014;87:318–27. http://dx.doi.org/10.1016/j.enconman.2014.07.014.
[16] Hosseinpour J, Sadeghi M, Chitsaz A, Ranjbar F, Rosen MA. Exergy assessment and optimization of a cogeneration system based on a solid oxide fuel cell integrated with a Stirling engine. Energy Convers Manag 2017;143:448–58.
[17] Xu H, Chen B, Tan P, Zhang H, Yuan J, Liu J, et al. Performance improvement of a direct carbon solid oxide fuel cell system by combining with a Stirling cycle. Energy 2017.
[18] Rokni M. Thermodynamic analysis of SOFC (solid oxide fuel cell)–Stirling hybrid plants using alternative fuels. Energy 2013;61:87–97. http://dx.doi.org/10.1016/j.energy.2013.06.001.
[19] Sammes N, Bove R, Stahl K. Phosphoric acid fuel cells: fundamentals and applications. Curr Opin Solid State Mater Sci 2004;8:372–8. http://dx.doi.org/10.1016/j.cossms.2005.01.001.
[20] Antolini E. The stability of molten carbonate fuel cell electrodes: a review of recent improvements. Appl Energy 2011;88:4274–93. http://dx.doi.org/10.1016/j.apenergy.2011.07.009.
[21] Basualdo MS, Feroldi D, Outbib R. PEM fuel cells with bio-ethanol processor systems: a multidisciplinary study of modelling, simulation, fault diagnosis and advanced control. Green Energy Technol 2012;87. http://dx.doi.org/10.1007/978-1-84996-184-4.
[22] Koponen J, Kosonen A, Ruuskanen V, Huoman K, Niemelä M, Ahola J. Control and energy efficiency of PEM water electrolyzers in renewable energy systems. Int J Hydrogen Energy 2017;2. http://dx.doi.org/10.1016/j.ijhydene.2017.10.056.
[23] Nami H, Mohammadkhani F, Ranjbar F. Utilization of waste heat from GTMHR for hydrogen generation via combination of organic Rankine cycles and PEM electrolysis. Energy Convers Manag 2016;127:589–98. http://dx.doi.org/10.1016/j.enconman.2016.09.043.
[24] Nami H, Akrami E. Analysis of a gas turbine based hybrid system by utilizing energy, exergy and exergoeconomic methodologies for steam, power and hydrogen production. Energy Convers Manag 2017;143:326–37. http://dx.doi.org/10.1016/j.enconman.2017.04.020.
[25] Moradi Nafchi F, Baniasadi E, Afshari E, Javani N. Performance assessment of a solar hydrogen and electricity production plant using high temperature PEM electrolyzer and energy storage. Int J Hydrogen Energy 2017:1–12. http://dx.doi.org/10.1016/j.ijhydene.2017.09.058.
[26] Boyaghchi FA, Chavoshi M, Sabeti V. Multi-generation system incorporated with PEM electrolyzer and dual ORC based on biomass gasification waste heat recovery: exergetic, economic and environmental impact optimizations. Energy 2018;145:38–51. http://dx.doi.org/10.1016/j.energy.2017.12.118.
[27] Ferrero D, Santarelli M. Investigation of a novel concept for hydrogen production by PEM water electrolysis integrated with multi-junction solar cells. Energy Convers Manag 2017;148:16–29. http://dx.doi.org/10.1016/j.enconman.2017.05.059.
[28] Sadeghi M, Mehr AS, Zar M, Santarelli M. Multi-objective optimization of a novel syngas fed SOFC power plant using a downdraft gasifier. Energy 2018;148:16–31. http://dx.doi.org/10.1016/j.energy.2018.01.114.
[29] Sharma S, Celebi AD, Maréchal F. Robust multi-objective optimization of gasifier and solid oxide fuel cell plant for electricity production using wood. Energy 2017;137:811–22. http://dx.doi.org/10.1016/j.energy.2017.04.146.
[30] Shamoushaki M, Ehyaei MA, Ghanatir F. Exergy, economic and environmental analysis and multi-objective optimization of a SOFC-GT power plant. Energy 2017;134:515–31. http://dx.doi.org/10.1016/j.energy.2017.06.058.
[31] Hajabdollahi Z, Fu PF. Multi-objective based configuration optimization of SOFC-GT cogeneration plant. Appl Therm Eng 2017;112:549–59. http://dx.doi.org/10.1016/j.applthermaleng.2016.10.103.
[32] Aminyavari M, Mamaghani AH, Shirazi A, Najafi B, Rinaldi F. Exergetic, economic, and environmental evaluations and multi-objective optimization of an internal-reforming SOFC-gas turbine cycle coupled with a Rankine cycle. Appl Therm Eng 2016;108:833–46. http://dx.doi.org/10.1016/j.applthermaleng.2016.07.180.
[33] Moran MJ, Shapiro HN, Boettner DD, Bailey MB. Fundamentals of engineering thermodynamics. John Wiley & Sons; 2010.
[34] Zainal ZA, Ali R, Lean CH, Seetharamu KN. Prediction of performance of a downdraft gasifier using equilibrium modeling for different biomass materials. Energy Convers Manag 2001;42:1499–515.
[35] Perry RH, Green DW, Maloney JO, Abbott MM, Ambler CM, Amero RC, et al. Perry's chemical engineers' handbook vol. 7. New York: McGraw-hill; 1997.
[36] Habibollahzade A, Houshfar E, Ashjaee M, Behzadi A, Gholamian E, Mehdizadeh H. Enhanced power generation through integrated renewable energy plants: solar chimney and waste-to-energy. Energy Convers Manag 2018;166:48–63. http://dx.doi.org/10.1016/j.enconman.2018.04.010.
[37] Gholamian E, Mahmoudi SMS, Zare V. Proposal, exergy analysis and optimization of a new biomass-based cogeneration system. Appl Therm Eng 2016;93:223–35. http://dx.doi.org/10.1016/j.applthermaleng.2015.09.095.
[38] Akkaya AV, Sahin B, Erdem HH. Exergetic performance coefficient analysis of a simple fuel cell system. Int J Hydrogen Energy 2007;32:4600–9.
[39] Yan Z, Zhao P, Wang J, Dai Y. Thermodynamic analysis of an SOFC–GT–ORC integrated power system with liquefied natural gas as heat sink. Int J Hydrogen Energy 2013;38:3352–63. http://dx.doi.org/10.1016/j.ijhydene.2012.12.101.
[40] Kuchonthara P, Bhattacharya S, Tsutsumi A. Energy recuperation in solid oxide fuel cell (SOFC) and gas turbine (GT) combined system. J Power Sources 2003;117:7–13. http://dx.doi.org/10.1016/S0378-7753(03)00009-0.
[41] Zhao H, Jiang T, Hou H. Performance analysis of the SOFC–CCHP system based on H2O/Li–Br absorption refrigeration cycle fueled by coke oven gas. Energy 2015;91:983–93. http://dx.doi.org/10.1016/j.energy.2015.08.087.
[42] Jia J, Li Q, Luo M, Wei L, Abudula A. Effects of gas recycle on performance of solid oxide fuel cell power systems. Energy 2011;36:1068–75. http://dx.doi.org/10.1016/j.energy.2010.12.001.
[43] Ni M, Leung MKH, Leung DYC. Energy and exergy analysis of hydrogen production by a proton exchange membrane (PEM) electrolyzer plant. Energy Convers Manag 2008;49:2748–56. http://dx.doi.org/10.1016/j.enconman.2008.03.018.
[44] Esmaili P, Dincer I, Naterer GF. Energy and exergy analyses of electrolytic hydrogen production with molybdenum-oxo catalysts. Int J Hydrogen Energy 2012;37:7365–72. http://dx.doi.org/10.1016/j.ijhydene.2012.01.076.
[45] Bejan A, Moran MJ. Thermal design and optimization. John Wiley & Sons; 1996.
[46] Wu C, Wang S sen, Feng X jia, Li J. Energy, exergy and exergoeconomic analyses of a combined supercritical CO_2 recompression Brayton/absorption refrigeration cycle. Energy Convers Manag 2017;148:360–77. http://dx.doi.org/10.1016/j.enconman.2017.05.042.
[47] Balli O, Aras H, Hepbasli A. Thermodynamic and thermoeconomic analyses of a trigeneration (TRIGEN) system with a gas-diesel engine: Part I – Methodology. Energy Convers Manag 2010;51:2252–9. http://dx.doi.org/10.1016/j.enconman.2010.03.021.
[48] Economic Indicators. Marshall&swift equipment cost index. Chem Eng 2011:72.
[49] Dinçer I, Rosen M, Ahmadi P. Optimization of energy systems. John Wiley & Sons;

2017.
[50] Assar M, Blumberg T, Morosuk T, Tsatsaronis G. Comparative exergoeconomic evaluation of two modern combined-cycle power plants. Energy Convers Manag 2016;153:616–26. http://dx.doi.org/10.1016/j.enconman.2017.10.036.
[51] Tao G, Armstrong T, Virkar A. Intermediate temperature solid oxide fuel cell (IT-SOFC) research and development activities at MSRI. In: Ninet annu ACERC&ICES Conf, Utah; 2005.
[52] Ioroi T, Yasuda K, Siroma Z, Fujiwara N, Miyazaki Y. Thin film electrocatalyst layer for unitized regenerative polymer electrolyte fuel cells. J Power Sources 2002;112:583–7. http://dx.doi.org/10.1016/S0378-7753(02)00466-4.
[53] Jarungthammachote S, Dutta A. Thermodynamic equilibrium model and second law analysis of a downdraft waste gasifier. Energy 2007;32:1660–9. http://dx.doi.org/10.1016/j.energy.2007.01.010.